Article:

eprints@whiterose.ac.uk
https://eprints.whiterose.ac.uk/

Wireless Friendliness Evaluation and Optimisation for Sandwich Building Materials as Reflectors

Yixin Zhang, *Member, IEEE*, Jiliang Zhang, *Senior Member, IEEE*,
Xiaoli Chu, *Senior Member, IEEE*, Jie Zhang, *Senior Member, IEEE*

Abstract—Sandwich-structured building materials are extensively used for energy saving, sound insulation and fire safety purposes. The electromagnetic (EM) waves incident on a sandwich building material will undergo complicated multiple reflections across all its layers and affect the indoor wireless performance in ways that are not yet fully understood. In this article, we establish a framework to evaluate and optimise the wireless friendliness of a sandwich building material. First, we derive and analyse the equivalent reflection coefficient of a sandwich building material. Then, based on a multipath channel model incorporating the line-of-sight (LOS) path and the reflections from the sandwich building material, we propose a metric for evaluating the wireless friendliness of a sandwich building material, i.e., the spatially averaged capacity over a room. Finally, we propose an iterative algorithm to maximise the spatially averaged capacity by jointly optimising the relative permittivity and thickness of each layer of the sandwich building material, while ensuring its mechanical and thermal insulation requirements. Numerical results show that the spatially averaged capacity can be increased by 25-42% via the joint optimisation of the relative permittivities and thickness of all layers of a sandwich building material.

Index Terms—Building wireless performance, channel model, electromagnetic wave propagation, multipath, permittivity, reflection, sandwich building material, wireless friendliness.

I. INTRODUCTION

A. Background and Motivation

The vast majority of wireless data traffic is predicted to take place in indoor environments, being it at home, in the office or in public buildings [1]–[4]. Meanwhile, users' demands for high-speed, reliable and ubiquitous indoor wireless services are continuing to increase [5]. Indoor wireless networks are envisioned as the fundamental enablers of smart buildings [6]. The indoor wireless performance is strongly affected by indoor wireless propagation environments, which are complicated due to diverse architectural design [7]–[10]. It has been shown that the properties of a building material [11]–[16] have a profound impact on indoor wireless performance.

To meet the increasing data traffic demand, indoor base stations (BSs) are equipped with large-scale multiple-input multiple-output (MIMO) antenna arrays [17], which are commonly deployed in the proximity of a wall for the sake of avoiding potential detrimental effects on the safety, functionality, and appearance of a room, e.g., in offices [18], hallways [19], conference rooms [20], and industrial mechanical rooms [21]. As a result, the interactions between the electromagnetic (EM) waves propagating indoors and the building materials are non-negligible in the analysis of indoor wireless performance [2], [6], [11].

Specifically, the EM waves emitted from the transmitter often experience complicated reflection processes, e.g., one-bounce reflection, with the intersecting physical objects before arriving at the receiver. The received signal power loss caused by reflections is jointly determined by the polarisation and the incident angle of the EM waves as well as the intrinsic EM and physical properties, e.g., the relative permittivity and thickness, of the building materials [20], [22], [23]. It is worth noting that a tiny variation in the relative permittivity and thickness of a building material will bring considerable changes in its reflection characteristics, and thus in the indoor wireless performance [12], [13]. Therefore, the selection/design of wireless-friendly building materials should be of prime concern during the building design and planning stage.

B. Literature review

Building materials used for walls, ceilings, floors, windows, and interior objects differ widely in ingredients. Traditional ingredients include: concrete, brick, plasterboard, wood, glass [24]–[29]. Concrete and brick are the typical components in building facades and the walls between rooms [24], [25]. Plasterboards are often used in interior walls to separate two rooms [26], [27]. Glass and wood are typically used for windows, doors and partitioners [28]. Besides, traditional ingredients used for heat insulation include: mineral wool, fibreglass, cellulose, polystyrene, and polyurethane foam (PUF) [30], [31]. The advantages of using these traditional ingredients of building materials include affordable price, readily available raw materials, and simple production method, which make them widely applied in constructions. However, since it is difficult and time-consuming to retrofit them or adjust their properties, the selection of building materials deserves careful consideration.

Practical building materials are generally multi-layer composite materials [27]. A typical concrete exterior wall of a residential building is a fabricated sandwich-like panel composing of two outlying concrete layers and a heat insulation layer between them [24], [25]. The interior structures of office buildings commonly adopt two wall types: a 3-layered structure with the air layer sandwiched between two plasterboard layers; or a 4-layered structure consisting of a plasterboard layer, an air layer, a heat insulator layer, and a concrete layer [27].

The conductivity, permittivity, and permeability are the three intrinsic EM properties of a building material [5]. However, for non-ionised and non-magnetic materials considered in this work, the conductivity and permittivity are the most important properties in response to an applied electric field, while the permeability is commonly approximated by the permeability of free space $\mu_0 = 4\pi \times 10^{-7}$ (N/A^2) [5], [25], [32]. That is because that a non-magnetic material does not exhibit strong magnetic response and hence the permeability hardly affects how a wave propagates through the material. Accordingly, the relative permittivity ε, a complex dimensionless constitutive parameter, is widely used to represent the EM property of a non-ionised, non-magnetic building material. The real part and imaginary part of ε are affected by the permittivity ϵ and the conductivity σ of the material, respectively [15], [32], i.e., $\varepsilon = (\epsilon - j\frac{\sigma}{\omega})/\epsilon_0$, where $\omega = 2\pi f$ denotes the angular frequency under frequency f and $\epsilon_0 = 8.854 \times 10^{-12}$ (F/m) denotes the permittivity of free space.

The relative permittivity of a building material may change with composition, moisture, and working frequency band. Taking concrete as an example, the three main components are cement, aggregate and water with a rough proportion of 1:7:2 [24, Table 1], while additional chemical admixtures are usually added to accelerate or slow down the hydration process and/or to increase the resistance against frost of hardened concrete. It has been shown, through measurements in [24], that the relative permittivity varies significantly among different concrete samples of various water-cement ratio, response to moisture, type and frequency band. For instance, comparing the S100B and SB45B concrete type [24, Table 2] with the same water-cement ratio of 0.7, the real parts of the relative permittivities are 4.89 and 5.72 in 4.5-19 GHz, respectively, and are 4.77 and 5.6 in 26-40 GHz band, respectively, while the imaginary parts of the relative permittivities are 0.22 and 0.22 in 4.5-19 GHz, respectively, and are 0.3 and 0.26 in 26-40 GHz band, respectively. As shown in [25, Fig. 7], among the 13 concrete samples measured in 7-13 GHz, the one of the highest water-cement ratio shows the largest variances in the real part of the relative permittivity measured on different days. Taking Sample 3 in [25, Table II] as an example, its real part of relative permittivity is, respectively, 4.89 being completely dried by oven, 10.25 being lifted up from water after being immersed in water for two days (i.e., the first measurement), 7.07 being 24 hours after the first measurement, and 5.94 being 72 hours after the first measurement. Moreover, the authors in [33] provided a dataset for various materials' dielectric properties based on the measurement of the complex relative permittivities and loss tangents of 20 common materi-

als (including but not limited to plastics, wood and wood-based materials, glass, gypsum plaster and plasterboard, brick, and concrete) over a very wide frequency band of 0.2-67 GHz in a complex indoor environment. It is shown that the frequency dependence of the material properties is well fitted by using a single-pole Cole-Cole model [34] for most materials.

The reflection characteristic of a sandwich building material is influenced by not only each individual layer's relative permittivity, but also each layer's thickness [32]. Considering the thermal characteristics and the design temperatures, the thickness of the heat insulation layer has to be specified according to the type of insulation materials [29, Table 1]. If the desired thickness is not commercially available, double or triple layers are applied with staggered joints [29, Sec. 2.1.5]. Increasingly stringent building regulations require good heat insulation of houses to ensure a high heating efficiency of buildings [26]. Furthermore, considering the mechanical performance, the total thickness of a sandwich building material is affected by its usage, e.g., load-bearing walls are usually much thicker than non-load bearing walls. For instance, the thickness of load-bearing wythe should be at least 75 mm thick [29, Sec. 2.1.6].

The "reflection coefficient" of a material describes how much of an incident EM wave is reflected by an impedance discontinuity in the transmission medium. Existing studies on the reflection coefficients of building materials are mostly through measurements and simulations. The authors in [35] measured the reflection coefficients of several material samples (PVC, wooden structures, plaster, mortar, concrete, etc.) in the frequency range between 8 and 12.5 GHz, and summarised that, in general, the amplitudes of the reflection coefficient slightly decrease with the frequency, while the phases decrease linearly with the frequency because the wavenumber increases as the wavelength decreases. The authors in [36] verified through simulations at 350 GHz that multiple reflections through a material result in higher spatial signal received power as compared to Fresnel reflections, and emphasised the importance of including multiple reflections from stratified building materials. The authors in [37] showed through simulations at 890 MHz that a multi-ray model (which considers multiple internal reflections) is more accurate than a single-ray model (which considers only a single reflection off the material surface) in modelling the reflection coefficients.

In summary, to the best of the authors' knowledge, the existing works mainly focus on measuring the signal attenuations [2], [20], [23]–[26], [28], relative permittivities [24], [25], [33], and reflection coefficients [35]–[37] of different sandwich building materials, missing the level of detail and diversity of a sandwich building material necessary for evaluating their impacts on the indoor wireless performance. It is worth noting that the measurement results are only applicable to the same building material or similar substitutes under the measured frequency band. There is a lack of methodology for evaluating the wireless friendliness of various sandwich building materials working in a wide frequency range. To fill this gap, it is necessary to establish the analytical relationship between the relative permittivity and thickness of each layer of a sandwich building material and the metrics of indoor

wireless performance.

To this end, in the framework of building wireless performance (BWP) [6], wireless friendliness has been proposed as a new metric for a building material to measure how it impacts wireless communications, which is determined by its constitutive EM and physical parameters [12]. In our previous work [12], [13], we have evaluated the wireless friendliness of a single-layer building material, and demonstrated that the relative permittivity and thickness of a single-layer building material need to be well configured to avoid the risk of reducing indoor wireless capacity. The evaluation metric proposed in [12] is the spatially averaged capacity of an indoor multipath channel that incorporates both the line-of-sight (LOS) path and the wall reflection (WR) path. To facilitate a fast and simple approach, the evaluation schemes in [13] adopt the spatially averaged logarithmic eigenvalue sum (LES) and spatially averaged logarithmic eigenvalue product (LEP) of a two-ray channel that includes the LOS path and the WR path as metrics. Nonetheless, how the EM and physical parameters of a sandwich building material influence indoor wireless performance, which is an important prerequisite for evaluating and optimising the wireless friendliness of sandwich building materials, has not been sufficiently studied.

C. Contributions

In this work, we focus on the wireless friendliness evaluation and optimisation of sandwich building materials as reflectors, taking the typical interior structures of office buildings as examples [27]. As far as we know, this is the first attempt to bridge the EM and physical parameters of a sandwich building material and the indoor wireless performance, so as to provide guidance on the design and optimisation of a sandwich building material for maximising its wireless friendliness and thus pave the way for future wireless-friendly architectural design.

The contributions of this work are summarised as follows:

- We derive and analyse the equivalent reflection coefficient while considering multiple internal reflections between layers of the sandwich building materials that are widely used in office buildings, for both transverse electric (TE) and transverse magnetic (TM) polarised incident EM waves. The constitutive terms of the equivalent reflection coefficient are explained with their physical meaning.
- We compare the downlink capacities from the BS to a typical user equipment (UE) based on three different channel models that take the reflections from the surrounding sandwich building materials into account: (i) the 5-ray model where the LOS path and the 4 WR paths from the 4 surrounding walls are determined; (ii) the 2-ray model where the LOS path and the WR path from the closest wall to the BS are taken as deterministic components, while the other multipath components (MPCs) are modelled as independent and identically distributed (i.i.d.) complex Gaussian variables scaled by the sum power of the 3 WR paths from the 3 farther walls; and (iii) the 1-ray model where the LOS path is the only deterministic component, while the other MPCs are

modelled as i.i.d complex Gaussian variables scaled by the sum power of the 4 WR paths from the 4 surrounding walls. Among the above three models, the 5-ray model is the most realistic model for a rectangular room. In terms of the downlink capacity spatially distributed in the considered room, we find that the 2-ray model leads to an accuracy very close to that of the 5-ray model while offering a better analytical tractability, i.e., a closed-form expression of the downlink capacity. Hence, we use the spatially averaged capacity [12] based on the 2-ray model as the metric for evaluating the wireless friendliness of a sandwich building material.

- We formulate an optimisation problem to maximise the spatially averaged capacity over a typical rectangular room by jointly optimising the relative permittivities and thickness of all layers of a sandwich building material, while ensuring its mechanical and thermal insulation requirements. An iterative algorithm is proposed to solve the problem and obtain the optimal values of the relative permittivity and thickness of each layer. Our numerical results show that the maximisation of the spatially averaged capacity based on the 2-ray model leads to the same optimal values of the relative permittivity and thickness of each layer for a sandwich building material as those obtained based on the 5-ray model.
- Based on the analytical and simulation results, we find that the spatially averaged capacity can be enhanced by 25-42% via a joint design of the relative permittivity and thickness of all layers of a sandwich building material, compared with the benchmark sandwich building material that adopts the relative permittivities given in ITU recommendations and the typical thickness.

The rest of the article is organized as follows. In Section II, we provide the expressions for the equivalent reflection coefficient of sandwich building materials, and plot its amplitude versus the incident angle for the TE and TM polarised EM waves. In Section III, we compare the downlink capacities from the BS to the UE based on three multipath channel models and adopt the spatially averaged capacity based on the 2-ray channel model as the metric to evaluate the wireless friendliness of a sandwich building material. In Section IV, we formulate the wireless friendliness optimisation problem that aims to maximise the spatially averaged capacity, propose an iterative algorithm to solve it, and present the simulation results of the proposed algorithm. Finally, the conclusion of this article is presented in Section V.

II. REFLECTION CHARACTERISTICS OF SANDWICH BUILDING MATERIALS

The structure of an M-layered sandwich building material is shown in Fig. 1(a), where for $m \in \{1, 2, ..., M\}$, ε_m and d_m denote the complex relative permittivity and thickness of the mth layer, respectively, Z_0 and Z_m denote the wave impedance in the air and in the mth layer, respectively, $\varepsilon_0 = 1$ and θ_0 denote the relative permittivity of the air and the incident angle in the air, respectively.

We adopt the two typical multi-layered interior wall models for office buildings [27]. In Fig. 1(b), wall A is a 4-layerd
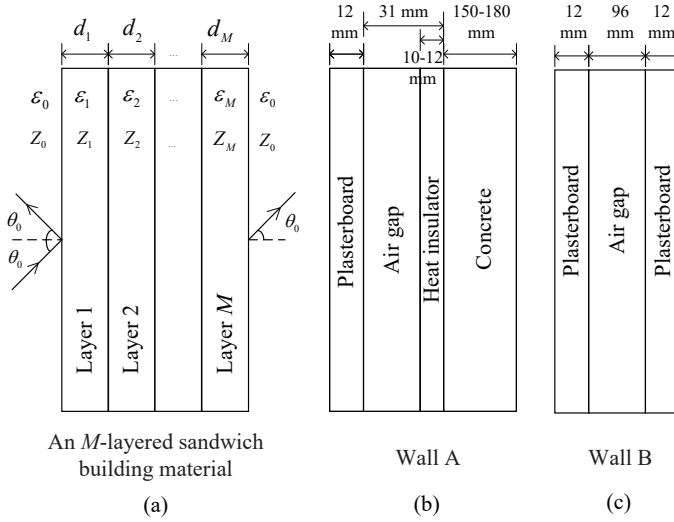
Fig. 1. Structure of (a) an M-layered sandwich building material, (b) wall A, and (c) wall B.

(a) An example of $L_{0,0,0}(\delta_1, \delta_2, \delta_3)$

(b) An example of $L_{0,1,0}(\delta_1, \delta_2, \delta_3)$

(c) An example of $L_{1,0,1}(\delta_1, \delta_2, \delta_3)$
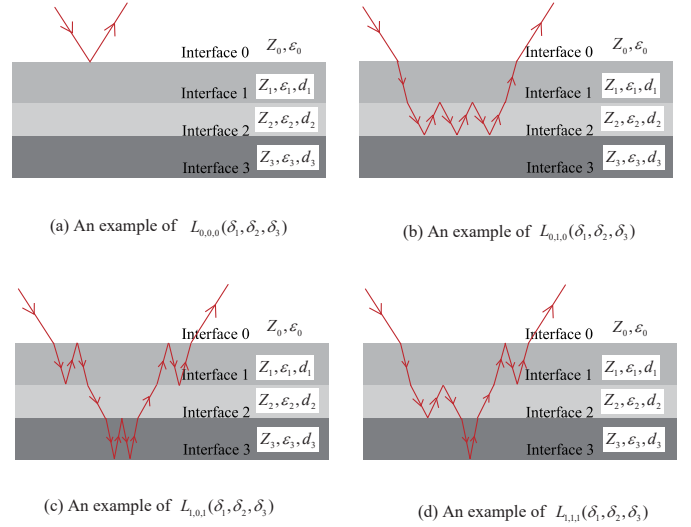
(d) An example of $L_{1,1,1}(\delta_1, \delta_2, \delta_3)$

Fig. 2. Illustration for the examples of $L_{X_1,X_2,X_3}(\delta_1, \delta_2, \delta_3)$ to show the multiple reflections off the 4 interfaces of a 3-layered sandwich building material.

concrete wall covered with a heat insulator, an air gap, and a plasterboard from the inside out. The thickness of the heat insulator and the air gap sums up to 31 mm. The plasterboard layer is of 12 mm in thickness, and the concrete layer is between 150 and 180 mm in thickness. The heat insulator layer is assumed to be filled with PUF. In Fig. 1(c), wall B presents a symmetric hollow plasterboard wall, where the air layer of 96 mm is sandwiched between two plasterboard layers, each of 12 mm thickness.

The wave impedance is dependent on the incidence polarisation [32]. Given the TE polarisation or TM polarisation of the incident electric field, Z_0 is given by

$$Z_0 = \begin{cases} \frac{120\pi}{\sqrt{1-\sin^2\theta_0}}, & \text{TE polarisation,} \\ 120\pi\sqrt{1-\sin^2\theta_0}, & \text{TM polarisation.} \end{cases} \quad (1)$$

and Z_m $(m = 1, ..., M)$ is given by

$$Z_m = \begin{cases} \frac{120\pi}{\sqrt{\varepsilon_m-\sin^2\theta_0}}, & \text{TE polarisation,} \\ \frac{120\pi\sqrt{\varepsilon_m-\sin^2\theta_0}}{\varepsilon_m}, & \text{TM polarisation.} \end{cases} \quad (2)$$

A. Equivalent reflection coefficient

Following [32, Annex 2], the equivalent reflection coefficient considering multiple internal reflections between layers for a 3-layered building material is given by

$$\Gamma = \frac{R_1}{R_2}, \quad (3)$$

where R_1 and R_2 are given as

$$R_1 = jL_{0,0,1}(\delta_1, \delta_2, \delta_3)\left(\frac{Z_3}{Z_0} - \frac{Z_0}{Z_3}\right)$$
$$+ jL_{0,1,0}(\delta_1, \delta_2, \delta_3)\left(\frac{Z_2}{Z_0} - \frac{Z_0}{Z_2}\right)$$
$$+ jL_{1,0,0}(\delta_1, \delta_2, \delta_3)\left(\frac{Z_1}{Z_0} - \frac{Z_0}{Z_1}\right)$$
$$+ jL_{1,1,1}(\delta_1, \delta_2, \delta_3)\left(\frac{Z_2Z_0}{Z_1Z_3} - \frac{Z_1Z_3}{Z_2Z_0}\right),$$

$$R_2 = 2L_{0,0,0}(\delta_1, \delta_2, \delta_3) - jL_{1,1,1}(\delta_1, \delta_2, \delta_3)\left(\frac{Z_2Z_0}{Z_1Z_3} + \frac{Z_1Z_3}{Z_2Z_0}\right)$$
$$- 2\frac{Z_1}{Z_2}L_{1,1,0}(\delta_1, \delta_2, \delta_3) + jL_{0,1,0}(\delta_1, \delta_2, \delta_3)\left(\frac{Z_2}{Z_0} + \frac{Z_0}{Z_2}\right)$$
$$- 2\frac{Z_2}{Z_3}L_{0,1,1}(\delta_1, \delta_2, \delta_3) + jL_{1,0,0}(\delta_1, \delta_2, \delta_3)\left(\frac{Z_1}{Z_0} + \frac{Z_0}{Z_1}\right)$$
$$- 2\frac{Z_1}{Z_3}L_{1,0,1}(\delta_1, \delta_2, \delta_3) + jL_{0,0,1}(\delta_1, \delta_2, \delta_3)\left(\frac{Z_3}{Z_0} + \frac{Z_0}{Z_3}\right).$$

in which

$$L_{\{X_1,X_2,...,X_M\}}(\delta_1, \delta_2, ...\delta_M) = \prod_{m=1}^{M} \cos\left(\delta_m - \frac{\pi}{2}X_m\right), \quad (4)$$

where $X_m \in \{0, 1\}$ is a binary variable,

$$\delta_m = v_m d_m \quad (5)$$

denotes the phase rotation of the EM wave in the mth layer,

$$v_m = k\sqrt{\varepsilon_m - \sin^2\theta_0} \quad (6)$$

denotes the propagation constant in the direction perpendicular to the mth layer, μ and $k = \frac{2\pi}{\mu}$ denotes the wavelength and the wavenumber of EM waves in the air, receptively.

As shown in (4)-(6), $L_{X_1,X_2,...,X_M}(\delta_1, \delta_2, ...\delta_M)$ indicates that if $X_m = 1$, $\forall m \in \{1, 2, ..., M\}$, an internal reflection occurs off the mth layer; and if $X_m = 0$, then no internal reflection occurs off the mth layer. For example, $L_{1,1,1}(\delta_1, \delta_2, \delta_3)$ indicates that a portion of the incident wave is reflected back through internal reflections off each of the three layers. For better understanding, the examples of the multiple internal reflections off the 4 interfaces of a 3-layered sandwich building material are illustrated in Fig. 2. As a result, the value of $L_{X_1,X_2,...,X_M}(\delta_1, \delta_2, ...\delta_M)$ determined by the right-hand side of (4) gives the total phase rotation of the EM wave imposed by the M-layered sandwich building material.

For a symmetric 3-layered structure, such as wall B shown in Fig. 1(c), subject to $d_1 = d_3$, $\varepsilon_1 = \varepsilon_3$, $\varepsilon_2 = \varepsilon_0 = 1$, $\delta_2 = kd_2\sqrt{1-\sin^2\theta_0}$, $Z_2 = Z_0$, the equivalent reflection coefficient considering multiple internal reflections between layers is given by

$$\Gamma_{\mathrm{B}} = \frac{B_1}{B_2}, \tag{7}$$

where B_1 and B_2 are given as

$$B_1 = j\sin(2\delta_1)\cos(\delta_2)\left(\frac{Z_1}{Z_0} - \frac{Z_0}{Z_1}\right)$$
$$+ j\sin^2(\delta_1)\sin(\delta_2)\left(\frac{Z_0^2}{Z_1^2} - \frac{Z_1^2}{Z_0^2}\right),$$

$$B_2 = 2\cos(2\delta_1)\cos(\delta_2) + j\exp(j\delta_2)\sin(2\delta_1)\left(\frac{Z_1}{Z_0} + \frac{Z_0}{Z_1}\right)$$
$$+ j2\cos^2(\delta_1)\sin(\delta_2) - j\sin^2(\delta_1)\sin(\delta_2)\left(\frac{Z_0^2}{Z_1^2} + \frac{Z_1^2}{Z_0^2}\right),$$

The equivalent reflection coefficient considering multiple internal reflections between layers for a 4-layered building material is given by

$$\Gamma' = \frac{G_1}{G_2}, \tag{8}$$

where G_1 and G_2 are given at the bottom of next page.

For the 4-layered wall A in Fig. 1(b), subject to $\varepsilon_2 = \varepsilon_0 = 1$, $\delta_2 = kd_2\sqrt{1-\sin^2\theta_0}$, $Z_2 = Z_0$, the equivalent reflection coefficient considering multiple internal reflections between layers is simplified as

$$\Gamma_{\mathrm{A}} = \frac{A_1}{A_2}, \tag{9}$$

where A_1 and A_2 are given at the bottom of next page.

By observing the equivalent reflection coefficients in (3) and (8) for a 3-layered or 4-layered building material, respectively, we find that the equivalent reflection coefficient of a sandwich building material is a fraction, where both the numerator and the denominator are complex. Specifically,

$$G_1 = jL_{0,0,0,1}(\delta_1,\delta_2,\delta_3,\delta_4)\left(\frac{Z_4}{Z_0} - \frac{Z_0}{Z_4}\right) + jL_{0,0,1,0}(\delta_1,\delta_2,\delta_3,\delta_4)\left(\frac{Z_3}{Z_0} - \frac{Z_0}{Z_3}\right) + jL_{0,1,0,0}(\delta_1,\delta_2,\delta_3,\delta_4)\left(\frac{Z_2}{Z_0} - \frac{Z_0}{Z_2}\right)$$
$$+ jL_{1,0,0,0}(\delta_1,\delta_2,\delta_3,\delta_4)\left(\frac{Z_1}{Z_0} - \frac{Z_0}{Z_1}\right) + jL_{0,1,1,1}(\delta_1,\delta_2,\delta_3,\delta_4)\left(\frac{Z_3Z_0}{Z_2Z_4} - \frac{Z_2Z_4}{Z_3Z_0}\right) + jL_{1,0,1,1}(\delta_1,\delta_2,\delta_3,\delta_4)\left(\frac{Z_3Z_0}{Z_1Z_4} - \frac{Z_1Z_4}{Z_3Z_0}\right)$$
$$+ jL_{1,1,0,1}(\delta_1,\delta_2,\delta_3,\delta_4)\left(\frac{Z_2Z_0}{Z_1Z_4} - \frac{Z_1Z_4}{Z_2Z_0}\right) + jL_{1,1,1,0}(\delta_1,\delta_2,\delta_3,\delta_4)\left(\frac{Z_2Z_0}{Z_3Z_1} - \frac{Z_3Z_1}{Z_2Z_0}\right),$$

$$G_2 = 2L_{0,0,0,0}(\delta_1,\delta_2,\delta_3,\delta_4) - 2L_{1,1,0,0}(\delta_1,\delta_2,\delta_3,\delta_4)\frac{Z_1}{Z_2} - 2L_{1,0,1,0}(\delta_1,\delta_2,\delta_3,\delta_4)\frac{Z_1}{Z_3} - 2L_{1,0,0,1}(\delta_1,\delta_2,\delta_3,\delta_4)\frac{Z_1}{Z_4}$$
$$- 2L_{0,1,1,0}(\delta_1,\delta_2,\delta_3,\delta_4)\frac{Z_2}{Z_3} - 2L_{0,1,0,1}(\delta_1,\delta_2,\delta_3,\delta_4)\frac{Z_2}{Z_4} - 2L_{0,0,1,1}(\delta_1,\delta_2,\delta_3,\delta_4)\frac{Z_3}{Z_4} + 2L_{1,1,1,1}(\delta_1,\delta_2,\delta_3,\delta_4)\frac{Z_1Z_3}{Z_2Z_4}$$
$$+ jL_{0,0,0,1}(\delta_1,\delta_2,\delta_3,\delta_4)\left(\frac{Z_4}{Z_0} + \frac{Z_0}{Z_4}\right) + jL_{0,0,1,0}(\delta_1,\delta_2,\delta_3,\delta_4)\left(\frac{Z_3}{Z_0} + \frac{Z_0}{Z_3}\right) + jL_{0,1,0,0}(\delta_1,\delta_2,\delta_3,\delta_4)\left(\frac{Z_2}{Z_0} + \frac{Z_0}{Z_2}\right)$$
$$+ jL_{1,0,0,0}(\delta_1,\delta_2,\delta_3,\delta_4)\left(\frac{Z_1}{Z_0} + \frac{Z_0}{Z_1}\right) - jL_{0,1,1,1}(\delta_1,\delta_2,\delta_3,\delta_4)\left(\frac{Z_3Z_0}{Z_2Z_4} + \frac{Z_2Z_4}{Z_3Z_0}\right) - jL_{1,0,1,1}(\delta_1,\delta_2,\delta_3,\delta_4)\left(\frac{Z_3Z_0}{Z_1Z_4} + \frac{Z_1Z_4}{Z_3Z_0}\right)$$
$$- jL_{1,1,0,1}(\delta_1,\delta_2,\delta_3,\delta_4)\left(\frac{Z_2Z_0}{Z_1Z_4} + \frac{Z_1Z_4}{Z_2Z_0}\right) - jL_{1,1,1,0}(\delta_1,\delta_2,\delta_3,\delta_4)\left(\frac{Z_2Z_0}{Z_3Z_1} + \frac{Z_3Z_1}{Z_2Z_0}\right).$$

$$A_1 = jL_{0,0,0,1}(\delta_1,\delta_2,\delta_3,\delta_4)\left(\frac{Z_4}{Z_0} - \frac{Z_0}{Z_4}\right) + jL_{0,0,1,0}(\delta_1,\delta_2,\delta_3,\delta_4)\left(\frac{Z_3}{Z_0} - \frac{Z_0}{Z_3}\right) + jL_{1,0,0,0}(\delta_1,\delta_2,\delta_3,\delta_4)\left(\frac{Z_1}{Z_0} - \frac{Z_0}{Z_1}\right)$$
$$+ jL_{0,1,1,1}(\delta_1,\delta_2,\delta_3,\delta_4)\left(\frac{Z_3}{Z_4} - \frac{Z_4}{Z_3}\right) + jL_{1,0,1,1}(\delta_1,\delta_2,\delta_3,\delta_4)\left(\frac{Z_3Z_0}{Z_1Z_4} - \frac{Z_1Z_4}{Z_3Z_0}\right)$$
$$+ jL_{1,1,0,1}(\delta_1,\delta_2,\delta_3,\delta_4)\left(\frac{Z_0^2}{Z_1Z_4} - \frac{Z_1Z_4}{Z_0^2}\right) + jL_{1,1,1,0}(\delta_1,\delta_2,\delta_3,\delta_4)\left(\frac{Z_0^2}{Z_3Z_1} - \frac{Z_3Z_1}{Z_0^2}\right),$$

$$A_2 = 2L_{0,0,0,0}(\delta_1,\delta_2,\delta_3,\delta_4) - 2L_{1,1,0,0}(\delta_1,\delta_2,\delta_3,\delta_4)\frac{Z_1}{Z_0} - 2L_{1,0,1,0}(\delta_1,\delta_2,\delta_3,\delta_4)\frac{Z_1}{Z_3} - 2L_{1,0,0,1}(\delta_1,\delta_2,\delta_3,\delta_4)\frac{Z_1}{Z_4}$$
$$- 2L_{0,1,1,0}(\delta_1,\delta_2,\delta_3,\delta_4)\frac{Z_0}{Z_3} - 2L_{0,1,0,1}(\delta_1,\delta_2,\delta_3,\delta_4)\frac{Z_0}{Z_4} - 2L_{0,0,1,1}(\delta_1,\delta_2,\delta_3,\delta_4)\frac{Z_3}{Z_4} + 2L_{1,1,1,1}(\delta_1,\delta_2,\delta_3,\delta_4)\frac{Z_1Z_3}{Z_0Z_4}$$
$$+ jL_{0,0,0,1}(\delta_1,\delta_2,\delta_3,\delta_4)\left(\frac{Z_4}{Z_0} + \frac{Z_0}{Z_4}\right) + jL_{0,0,1,0}(\delta_1,\delta_2,\delta_3,\delta_4)\left(\frac{Z_3}{Z_0} + \frac{Z_0}{Z_3}\right) + j2L_{0,1,0,0}(\delta_1,\delta_2,\delta_3,\delta_4)$$
$$+ jL_{1,0,0,0}(\delta_1,\delta_2,\delta_3,\delta_4)\left(\frac{Z_1}{Z_0} + \frac{Z_0}{Z_1}\right) - jL_{0,1,1,1}(\delta_1,\delta_2,\delta_3,\delta_4)\left(\frac{Z_3}{Z_4} + \frac{Z_4}{Z_3}\right) - jL_{1,0,1,1}(\delta_1,\delta_2,\delta_3,\delta_4)\left(\frac{Z_3Z_0}{Z_1Z_4} + \frac{Z_1Z_4}{Z_3Z_0}\right)$$
$$- jL_{1,1,0,1}(\delta_1,\delta_2,\delta_3,\delta_4)\left(\frac{Z_0^2}{Z_1Z_4} + \frac{Z_1Z_4}{Z_0^2}\right) - jL_{1,1,1,0}(\delta_1,\delta_2,\delta_3,\delta_4)\left(\frac{Z_0^2}{Z_3Z_1} + \frac{Z_3Z_1}{Z_0^2}\right).$$

TABLE I
THE NUMERATORS AND DENOMINATORS OF THE EQUIVALENT REFLECTION COEFFICIENTS CONSIDERING MULTIPLE INTERNAL REFLECTIONS FOR
3-LAYERED OR 4-LAYERED SANDWICH BUILDING MATERIALS

		3-layered sandwich building materials	4-layered sandwich building materials
Numerator	Real parts	——	——
	Imaginary parts	$\sum\limits_{\substack{\forall a=1,2,3 \\ s.t.X_a=0,\ X_1+X_2+X_3=1, \\ X_1,X_2,X_3\in\{0,1\}}} L_{X_1,X_2,X_3}\left(\frac{Z_a}{Z_0}-\frac{Z_0}{Z_a}\right)$	$\sum\limits_{\substack{\forall a=1,2,3,4 \\ s.t.X_a=0,\ X_1+X_2+X_3+X_4=1, \\ X_1,X_2,X_3,X_4\in\{0,1\}}} L_{X_1,X_2,X_3,X_4}\left(\frac{Z_a}{Z_0}-\frac{Z_0}{Z_a}\right)$
		$L_{1,1,1}\left(\frac{Z_2 Z_0}{Z_1 Z_3}-\frac{Z_1 Z_3}{Z_2 Z_0}\right)$	$\sum\limits_{\substack{\forall a=1,2,3,4,a<b<c \\ s.t.X_a=X_b=X_c=0,\ X_1+X_2+X_3+X_4=3, \\ X_1,X_2,X_3,X_4\in\{0,1\}}} L_{X_1,X_2,X_3,X_4}\left(\frac{Z_b Z_0}{Z_a Z_c}-\frac{Z_a Z_c}{Z_b Z_0}\right)$
Denominator		$2L_{0,0,0}$	$2L_{0,0,0,0}$
	Real parts	$\sum\limits_{\substack{\forall a,b=1,2,3,a<b \\ s.t.X_a=X_b=0,\ X_1+X_2+X_3=2, \\ X_1,X_2,X_3\in\{0,1\}}} -2L_{X_1,X_2,X_3}\frac{Z_a}{Z_b}$	$\sum\limits_{\substack{\forall a,b=1,2,3,4,a<b \\ s.t.X_a=X_b=0,\ X_1+X_2+X_3+X_4=2, \\ X_1,X_2,X_3,X_4\in\{0,1\}}} -2L_{X_1,X_2,X_3,X_4}\frac{Z_a}{Z_b}$
		——	$2L_{1,1,1,1}\frac{Z_1 Z_3}{Z_2 Z_4}$
	Imaginary parts	$\sum\limits_{\substack{\forall a=1,2,3 \\ s.t.X_a=0,\ X_1+X_2+X_3=1, \\ X_1,X_2,X_3\in\{0,1\}}} L_{X_1,X_2,X_3}\left(\frac{Z_a}{Z_0}+\frac{Z_0}{Z_a}\right)$	$\sum\limits_{\substack{\forall a=1,2,3,4 \\ s.t.X_a=0,\ X_1+X_2+X_3+X_4=1, \\ X_1,X_2,X_3,X_4\in\{0,1\}}} L_{X_1,X_2,X_3,X_4}\left(\frac{Z_a}{Z_0}+\frac{Z_0}{Z_a}\right)$
		$-L_{1,1,1}\left(\frac{Z_2 Z_0}{Z_1 Z_3}+\frac{Z_1 Z_3}{Z_2 Z_0}\right)$	$\sum\limits_{\substack{\forall a=1,2,3,4,a<b<c \\ s.t.X_a=X_b=X_c=0,\ X_1+X_2+X_3+X_4=3, \\ X_1,X_2,X_3,X_4\in\{0,1\}}} -L_{X_1,X_2,X_3,X_4}\left(\frac{Z_b Z_0}{Z_a Z_c}+\frac{Z_a Z_c}{Z_b Z_0}\right)$

the constitutive terms in the numerators and denominators of the equivalent reflection coefficients are summarised in Table I, where the $L_{X_1,X_2,...,X_M}$ function and the wave impedance Z_x (for $x = 1, 2, ...M$) are given in (4) and (1)-(2), respectively. Due to space limitation, we omit $(\delta_1, \delta_2, ...\delta_M)$ from $L_{X_1,X_2,...,X_M}(\delta_1, \delta_2, ...\delta_M)$ in Table I. The constitutive terms characterise the multiple reflections off the $M+1$ inner surfaces inside the M-layered sandwich building material. The wave impedance-dependent constitutive terms, e.g., $\left(\frac{Z_a}{Z_b}\right)$, $\left(\frac{Z_a}{Z_0} - \frac{Z_0}{Z_a}\right)$, and $\left(\frac{Z_b Z_0}{Z_a Z_c} - \frac{Z_a Z_c}{Z_b Z_0}\right)$ (for $a, b, c = 1, 2, ...M$), reveal which layers are involved in internal reflections of the transverse field through the M-layered sandwich building material. The phase rotation-dependent constitutive terms, i.e., $L_{X_1,X_2,...,X_M}(\delta_1, \delta_2, ...\delta_M)$, $\forall m \in \{1, 2, ..., M\}$, are jointly affected by the incident angle θ_0, the relative permittivity of each layer ε_m, and the thickness of each layer d_m [32].

B. Examples

The equivalent reflection coefficient amplitudes of wall A and wall B versus the incident angle are presented in Fig. 3 and Fig. 4, respectively. The relative permittivity of concrete, plasterboard, and PUF at 6 GHz are given in accordance with [30], [31], [32, Table III]. We can see that the analytical expressions of the equivalent reflection coefficient match well with the method given in ITU recommendations [32, Annex 2], which verifies the accuracy of (9) and (7).

We observe that the equivalent reflection coefficient amplitude of a sandwich material varies with the incident angle, which can be attributed to the interference among the EM waves reflected from different layers that changes with the incident angle. This variation with the incident angle becomes more dramatic for the 3-layered wall B than for the 4-layered wall A, which can be explained as follows. As shown in (4), the L function, which is a constitutive term in the numerator and denominator of the equivalent reflection coefficient, is a multiplicative of M sine functions of the phase rotation per layer δ_m ($m = 1, 2, ..., M$). Note that the value of each sine function is between 0 and 1. As M increases, the value of the L function varies less significantly with δ_m. Moreover, as shown in (5) and (6), δ_m decreases with the incident angle θ_0. Hence, the amplitude of the equivalent reflection coefficient of the 3-layered wall B varies more dramatically with the incident angle than the 4-layered wall A.

Meanwhile, different polarisations of the incident waves lead to different values of the equivalent reflection coefficient amplitude. For both wall A and wall B, the TE polarised incident waves will obtain a larger reflection coefficient amplitude as compared with the TM polarised incident waves.

Furthermore, we can see that the reflection coefficient amplitude for the TM polarised incident waves is significantly reduced at an incident angle of around $60°$. That is because $60°$ is the Brewster angle when the EM waves incident on the layer 1 from the air, i.e.,
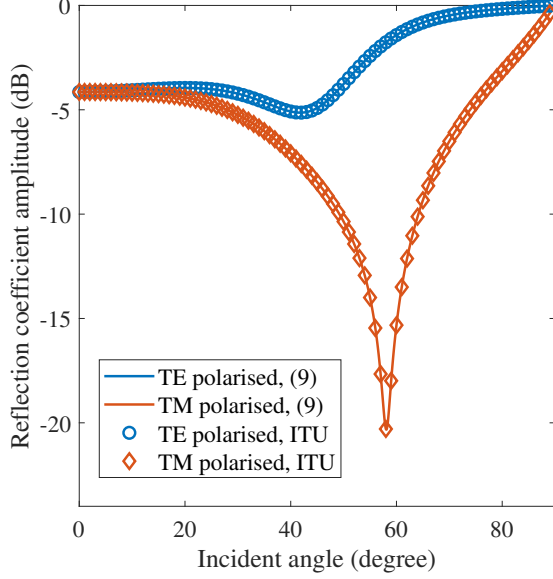
Fig. 3. Reflection coefficient amplitude for 4-layered wall A, where the incident wave is either TE or TM polarised, $\varepsilon_1 = 2.73 – j0.137$, $\varepsilon_3 = 1.3 – j0.3$, $\varepsilon_4 = 5.24 - j0.562$, $[d_1, d_2, d_3, d_4] = [12, 21, 10, 160]$ mm. The markers represent analytical values derived by (9) while the solid lines represent values derived by ITU recommendations [32, Annex 2].
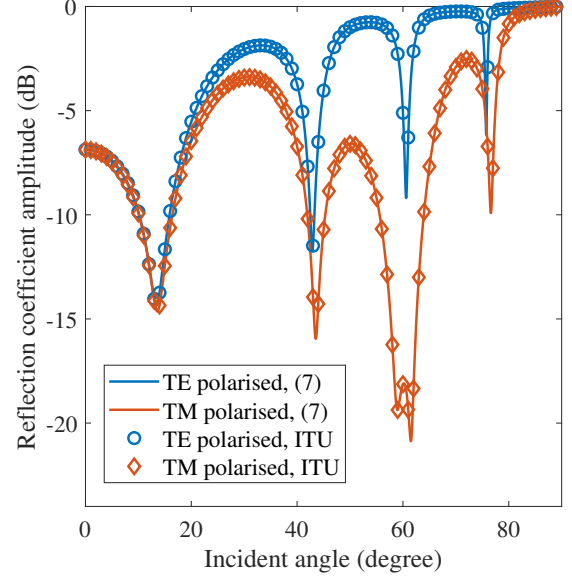

Fig. 4. Reflection coefficient amplitude for 3-layered wall B, where the incident wave is either TE or TM polarised, $\varepsilon_1 = \varepsilon_3 = 2.73 - j0.137$, $[d_1, d_2, d_3] = [12, 96, 12]$ mm. The markers represent analytical values derived by (7) while the solid lines represent values derived by ITU recommendations [32, Annex 2].

$$\theta_{\mathrm{B}} = \arctan\left(\sqrt{\frac{\varepsilon_{\mathrm{Layer\ 1}}}{\varepsilon_0}}\right),$$

At the Brewster angle, there is no reflection of parallel electric field. However, the Brewster angle does not affect the TE incident waves much, because realising an TE-polarisation Brewster effect requires a material with magnetic response, which is challenging for most practical non-magnetic building materials since the magnetic response of materials is extremely weak.

III. WIRELESS FRIENDLINESS EVALUATION FOR SANDWICH BUILDING MATERIALS

A. System model

The system model of an indoor LOS MIMO downlink in a rectangular room is shown in Fig. 5. The BS is placed on the centreline perpendicular to one of the walls with a small BS-wall distance D_0 m, and a typical UE is located at an arbitrary position in the room. The BS and the UE are both fitted with a uniform linear array (ULA) with the inter-antenna spacing of d_0 m, consisting of N_{T} and N_{R} antennas, respectively. The ULAs at the BS and at the UE are both assumed to be parallel to the wall closest to the BS. The four surrounding walls are made of the same M-layered sandwich building material defined by each layer's relative permittivity $\{\varepsilon_1, \varepsilon_2, ..., \varepsilon_M\}$ and thickness $\{d_1, d_2, ..., d_M\}$, as shown in Fig. 1.

As illustrated in Fig. 5, the channel model includes the LOS path and the 4 one-bounce WR paths from the 4 surrounding walls, which are denoted by $N_{\mathrm{R}} \times N_{\mathrm{T}}$ matrices $\mathbf{H}_1$, $\mathbf{H}_2$, $\mathbf{H}_3$, $\mathbf{H}_4$, and $\mathbf{H}_5$, respectively. Their corresponding UE location-specific path lengths, reflection coefficients, angles of departure (AoD), and angles of arrival (AoA) with respect to the

centre of the BS's ULA and the centre of UE's ULA are given by D_l, Γ_l, θ_{T_l}, and θ_{R_l}, respectively, for $l = 1, 2, 3, 4, 5$. Particularly, Γ_1 is set to 1 since the LOS path gain is not affected by the surrounding sandwich building materials. Γ_l (for $l = 2, 3, 4, 5$) denotes the equivalent reflection coefficient of the M-layered sandwich building material along the lth path, which is a function of the incident angle, i.e. θ_{I_l}, and the properties of the sandwich building material, i.e., $\{\varepsilon_1, \varepsilon_2, ..., \varepsilon_M\}$ and $\{d_1, d_2, ..., d_M\}$. For instance, the closed-form expressions of the equivalent reflection coefficient of a 3-layered or 4-layered sandwich building material are given in (3)-(9).

Following Friis' law, the $(n_{\mathrm{R}}, n_{\mathrm{T}})$-th element of $\mathbf{H}_1$, $\mathbf{H}_2$, $\mathbf{H}_3$, $\mathbf{H}_4$, and $\mathbf{H}_5$ are given, respectively, by

$$[\mathbf{H}_1]_{n_{\mathrm{R}},n_{\mathrm{T}}} = \frac{\mu\Gamma_1}{4\pi D_1} e^{-jkD_1 - j\left(n_{\mathrm{R}} - \frac{N_{\mathrm{R}}-1}{2}\right)k\beta_1 - j\left(n_{\mathrm{T}} - \frac{N_{\mathrm{T}}-1}{2}\right)k\alpha_1},$$

(10)

$$[\mathbf{H}_2]_{n_{\mathrm{R}},n_{\mathrm{T}}} = \frac{\mu\Gamma_2}{4\pi D_2} e^{-jkD_2 - j\left(n_{\mathrm{R}} - \frac{N_{\mathrm{R}}-1}{2}\right)k\beta_2 - j\left(n_{\mathrm{T}} - \frac{N_{\mathrm{T}}-1}{2}\right)k\alpha_2},$$

(11)

$$[\mathbf{H}_3]_{n_{\mathrm{R}},n_{\mathrm{T}}} = \frac{\mu\Gamma_3}{4\pi D_3} e^{-jkD_3 - j\left(n_{\mathrm{R}} - \frac{N_{\mathrm{R}}-1}{2}\right)k\beta_3 - j\left(n_{\mathrm{T}} - \frac{N_{\mathrm{T}}-1}{2}\right)k\alpha_3},$$

(12)

$$[\mathbf{H}_4]_{n_{\mathrm{R}},n_{\mathrm{T}}} = \frac{\mu\Gamma_4}{4\pi D_4} e^{-jkD_4 - j\left(n_{\mathrm{R}} - \frac{N_{\mathrm{R}}-1}{2}\right)k\beta_4 - j\left(n_{\mathrm{T}} - \frac{N_{\mathrm{T}}-1}{2}\right)k\alpha_4},$$

(13)

$$[\mathbf{H}_5]_{n_{\mathrm{R}},n_{\mathrm{T}}} = \frac{\mu\Gamma_5}{4\pi D_5} e^{-jkD_5 - j\left(n_{\mathrm{R}} - \frac{N_{\mathrm{R}}-1}{2}\right)k\beta_5 - j\left(n_{\mathrm{T}} - \frac{N_{\mathrm{T}}-1}{2}\right)k\alpha_5},$$

(14)

where $j = \sqrt{-1}$, $n_{\mathrm{T}} \in \{0, 1, ..., N_{\mathrm{T}} - 1\}$ and $n_{\mathrm{R}} \in \{0, 1, ..., N_{\mathrm{R}} - 1\}$ are the indices of transmit and receive antennas, respectively,

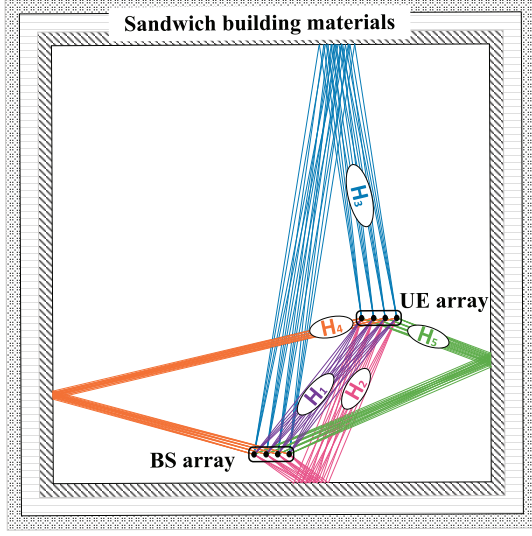$$\alpha_l = d_0 \cos\theta_{\mathrm{T}_l},$$

Fig. 5. The LOS path and the 4 one-bounce WR paths in a rectangular room.

$$\beta_l = d_0 \cos\theta_{\mathrm{R}_l},$$

for $l \in \{1,2,3,4,5\}$.

On the right-hand side of (10)-(14), $\frac{\mu}{4\pi D_l}$ follows the contemporary formula of Friis transmission equation, Γ_l (for $l = 2,3,4,5$) denotes the equivalent reflection co-efficient considering multiple internal reflections between layers of the M-layered sandwich building material, and $e^{-jkD_l - j\left(n_{\mathrm{R}} - \frac{N_{\mathrm{R}}-1}{2}\right)k\beta_l - j\left(n_{\mathrm{T}} - \frac{N_{\mathrm{T}}-1}{2}\right)k\alpha_l}$ gives the phase rotation imposed on the signal due to its propagation from the n_{T}th transmit antenna to the n_{R}th receive antenna along the lth path.

B. Comparison of Channel Models

In order to characterise the wireless friendliness of a sand-wich building material, an accurate and tractable channel model is required. In this subsection, we compare the following three channel models:

$$\mathbf{H}_{1\mathrm{ray}} = \mathbf{H_1} + \sqrt{P_1}\tilde{\mathbf{H}}, \quad P_1 = \sum_{l=2}^{5}\|\mathbf{H}_l\|^2, \qquad (15)$$

$$\mathbf{H}_{2\mathrm{ray}} = \mathbf{H_1} + \mathbf{H_2} + \sqrt{P_2}\tilde{\mathbf{H}}, \quad P_2 = \sum_{l=3}^{5}\|\mathbf{H}_l\|^2, \qquad (16)$$

$$\mathbf{H}_{5\mathrm{ray}} = \sum_{l=1}^{5}\mathbf{H}_l, \qquad (17)$$

where $\|\cdot\|$ denotes the F-norm of a matrix, $\tilde{\mathbf{H}}$ is a N_{R}-by-N_{T} matrix, and each element of $\tilde{\mathbf{H}}$ is an independent and identically distributed (i.i.d.) complex Gaussian random variable with zero-mean and unit-variance. Note that $\mathbf{H}_{1\mathrm{ray}}$ is based on the Rician fading model that characterises only the LOS path as the deterministic component, $\mathbf{H}_{2\mathrm{ray}}$ is the multipath channel model proposed in [12] that characterises both the LOS path and the WR path from BS's closest wall as

the deterministic components, while $\mathbf{H}_{5\mathrm{ray}}$ is the ray tracing model characterising the LOS path and all 4 WR paths as deterministic components. In theory, $\mathbf{H}_{5\mathrm{ray}}$ should be more accurate than $\mathbf{H}_{1\mathrm{ray}}$ or $\mathbf{H}_{2\mathrm{ray}}$.

The downlink capacities from the BS to the UE based on $\mathbf{H}_{1\mathrm{ray}}$, $\mathbf{H}_{2\mathrm{ray}}$, and $\mathbf{H}_{5\mathrm{ray}}$ are denoted by $C_{1\mathrm{ray}}$, $C_{2\mathrm{ray}}$, and $C_{5\mathrm{ray}}$, respectively, and are calculated using

$$C_{\mathrm{MD}} = \mathbb{E}\left[\log_2 \det\left(\mathbf{I} + \frac{\rho}{N_{\mathrm{T}}}\mathbf{H}_{\mathrm{MD}}\mathbf{H}_{\mathrm{MD}}{}^{\dagger}\right)\right], \qquad (18)$$

where the subscript "MD" can be "1ray" or "2ray" or "5ray", ρ denotes the transmit signal-to-noise ratio (SNR), and $\mathbb{E}(\cdot)$ denotes the expectation of a random variable.

In the following, we numerically evaluate the channel capacity at 6 GHz for various UE locations in a 10 m × 10 m room, following a typical indoor small office scenario defined in [38]. The UE and BS each employ a ULA consisting of 4 omni-directional antennas, each with a unit gain and the inter-antenna spacing of half wavelength. The transmit SNR is assumed to be 60 dB [39].

Fig. 6 and Fig. 7 show the downlink capacity based on $\mathbf{H}_{1\mathrm{ray}}$, $\mathbf{H}_{2\mathrm{ray}}$ and $\mathbf{H}_{5\mathrm{ray}}$ and their difference for wall A or wall B being the building material of the four surrounding walls. We can see that $C_{2\mathrm{ray}}$ and $C_{5\mathrm{ray}}$ are very close to each other, and their difference is less than 1 bit/s/Hz in most UE locations. While the difference between $C_{2\mathrm{ray}}$ and $C_{1\mathrm{ray}}$ or between $C_{5\mathrm{ray}}$ and $C_{1\mathrm{ray}}$ is relatively high, e.g., up to 15 bit/s/Hz in certain UE locations. Accordingly, $\mathbf{H}_{2\mathrm{ray}}$ can be used as a simple substitute of $\mathbf{H}_{5\mathrm{ray}}$ for evaluating the downlink capacity. The reason behind this is that given the BS deployed very close to a wall to the UE, the LOS path and the WR path from the closest wall to the UE have similar length, AoDs, and AoAs. Hence, the interference between these two paths would be much stronger than the interference between the LOS path and the WR path reflected from any of the other 3 walls farther away from the BS.

The above results show that the WR path reflected from the BS's closest wall has a remarkable impact on the indoor wireless capacity and should be characterised in the deterministic parts of the channel model, while the WR paths reflected from the other 3 walls can be incorporated as i.i.d components in the random parts of the channel model. Therefore, we propose to evaluate the wireless friendliness of a sandwich building material based on $\mathbf{H}_{2\mathrm{ray}}$ for simplicity and analytical tractability.

C. Evaluation Metric of Wireless Friendliness

$\mathbf{H}_{2\mathrm{ray}}$ can be rewritten as follows [12, (8)-(13)],

$$\mathbf{H} = \sqrt{\frac{K_0 S}{1 + K_0 S}}\eta\mathbf{H_1} + \sqrt{\frac{K_0 S}{1 + K_0 S}}\eta\mathbf{H_2} + \sqrt{\frac{1}{1 + K_0 S}}\tilde{\mathbf{H}}, \qquad (19)$$

where K_0 denotes the Rician factor defining the power ratio between the LOS component and MPCs, and is given by

$$K_0 = \frac{\|\mathbf{H_1}\|^2}{\|\mathbf{H_3}\|^2 + \|\mathbf{H_4}\|^2 + \|\mathbf{H_5}\|^2} = \frac{\frac{1}{d_1^2}}{\frac{|\Gamma_3|^2}{d_3^2} + \frac{|\Gamma_4|^2}{d_4^2} + \frac{|\Gamma_5|^2}{d_5^2}}, \qquad (20)$$
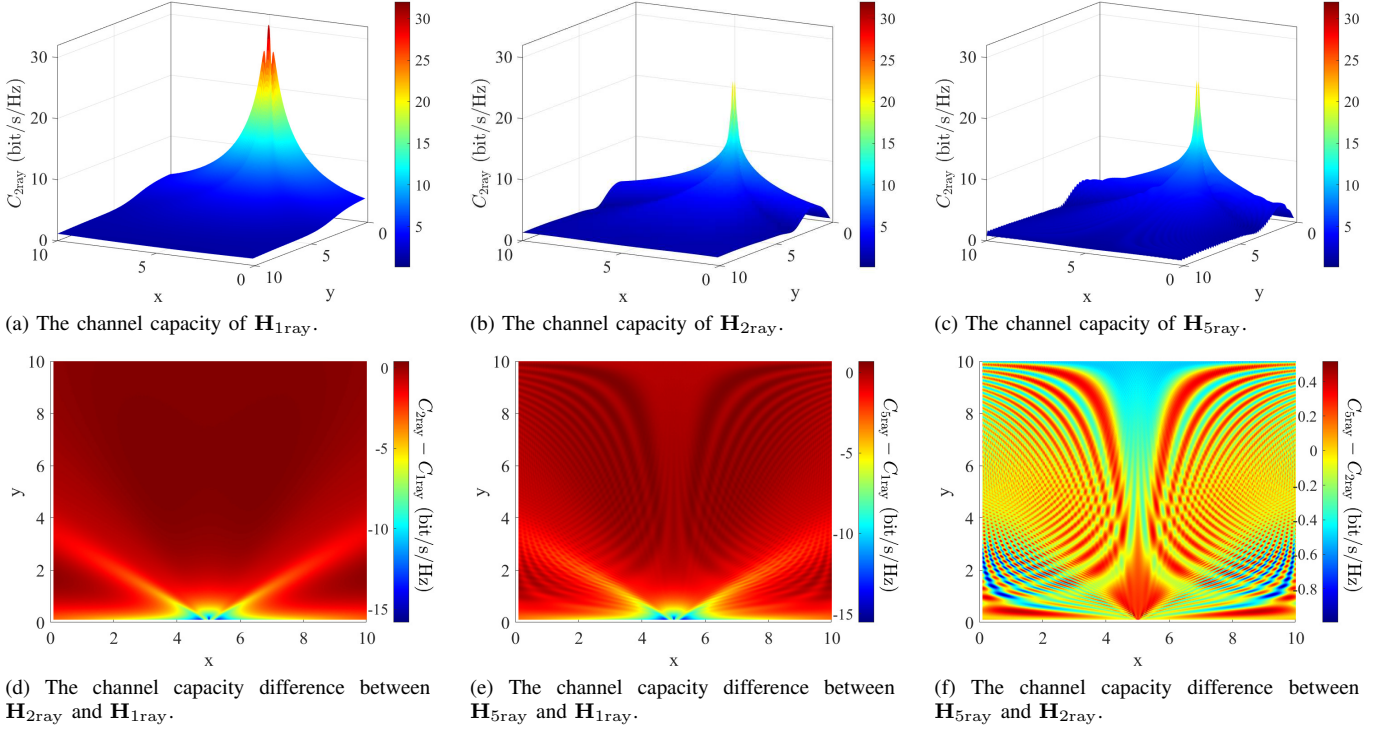
Fig. 6. Comparisons of the channel capacity of $\mathbf{H}_{1\mathrm{ray}}$, $\mathbf{H}_{2\mathrm{ray}}$, and $\mathbf{H}_{5\mathrm{ray}}$ for wall A, , where the incident wave is TE polarised, $\varepsilon_1 = 2.73 - j0.137$, $\varepsilon_3 = 1.3 - j0.3$, $\varepsilon_4 = 5.24 - j0.562$, $[d_1, d_2, d_3, d_4] = [12, 21, 10, 160]$ mm, and $D_0 = 37.5$ mm.

$S \triangleq \frac{\|\mathbf{H_1}+\mathbf{H_2}\|^2}{\|\mathbf{H_1}\|^2}$ denotes the power ratio of the summation of $\mathbf{H_1}$ and $\mathbf{H_2}$ to $\mathbf{H_1}$ and is given by

$$S = \frac{D_1^2}{D_2^2}|\Gamma|^2 + \frac{2S_0 D_1}{N_\mathrm{T} N_\mathrm{R} D_2}\Re\left(\Gamma e^{-j2\pi \frac{D_2-D_1}{\mu}}\right) + 1, \quad (21)$$

$$S_0 = \frac{\sin\left(\frac{N_\mathrm{T}}{2}\left(\alpha_2 - \alpha_1\right)\right)}{\sin\left(\frac{1}{2}\left(\alpha_2 - \alpha_1\right)\right)} \frac{\sin\left(\frac{N_\mathrm{R}}{2}\left(\beta_2 - \beta_1\right)\right)}{\sin\left(\frac{1}{2}\left(\beta_2 - \beta_1\right)\right)},$$

and

$$\eta = \frac{\sqrt{N_\mathrm{R} N_\mathrm{T}}}{\|\mathbf{H_1} + \mathbf{H_2}\|}$$

denotes the normalisation parameter subject to

$$\mathbb{E}[\mathrm{Tr}\{\mathbf{HH}^\dagger\}] = N_\mathrm{R} N_\mathrm{T},$$

where $\mathrm{Tr}\left(\cdot\right)$ denotes the trace of a matrix.

Following our previous work [12], we adopt the spatially averaged capacity over a room as the metric for evaluating the wireless friendliness of the sandwich building material. We take $X \times Y$ sample points evenly distributed across the considered room, and calculate the spatially averaged capacity over it by

$$C_\mathrm{avg} = \frac{1}{XY}\sum_{a=1}^{X}\sum_{b=1}^{Y} C\left(x_a, y_b\right), \quad (22)$$

where x_a and y_b denote the coordinate values of the a-th sample point along the x axis and that of the b-th sample point along the y axis, respectively, $a \in \{1, 2, ..., X\}$, $b \in \{1, 2, ..., Y\}$, $C\left(x_a, y_b\right)$ in bit/s/Hz denotes the downlink capacity at the UE location $\left(x_a, y_b\right)$ and its closed-form expression is given in Appendix A following [12, Theroem 2]. Generally, a greater value of C_avg corresponds to a better wireless friendliness of the sandwich building material.

IV. WIRELESS FRIENDLINESS OPTIMISATION FOR SANDWICH BUILDING MATERIALS

As the spatially averaged capacity in (22) is an effective metric for evaluating the wireless friendliness of a sandwich building material, the wireless friendliness of a sandwich material can be optimised by maximising the spatially averaged capacity. In this section, we formulate an optimization problem to maximise the spatially averaged capacity by optimising the properties of each layer, including the real part of relative permittivity, imaginary part of relative permittivity, and thickness, under the premise of ensuring the mechanical and thermal insulation requirements of the sandwich building material.

A. Problem formulation

For an M-layered building material, the optimisation problem is formulated as

$$\max_{\substack{\Re(\varepsilon_m),\Im(\varepsilon_m),d_m, \\ \text{for } m=1,2,...,M}} C_\mathrm{avg}$$

$$\begin{aligned} \text{s.t.} \quad &\Re(\varepsilon_m) \in \Upsilon_{\mathrm{type},m}, \text{ for } m = 1, 2, ..., M, \\ &\Im(\varepsilon_m) \in \Omega_{\mathrm{type},m}, \quad \text{for } m = 1, 2, ..., M, \\ &d_m \in \Xi_{\mathrm{type},m}, \text{ for } m = 1, 2, ..., M, \\ &\sum_{m=1}^{M} d_m \geq T_{\mathrm{type}}, \\ &\frac{1}{\sum_{m=1}^{M}\frac{d_m}{\kappa_{\mathrm{type},m}}} \leq U_{\mathrm{type}}. \end{aligned}$$

$$(23)$$

(a) The channel capacity of $\mathbf{H}_{1\text{ray}}$.

(b) The channel capacity of $\mathbf{H}_{2\text{ray}}$.

(c) The channel capacity of $\mathbf{H}_{5\text{ray}}$.

(d) The channel capacity difference between $\mathbf{H}_{2\text{ray}}$ and $\mathbf{H}_{1\text{ray}}$.

(e) The channel capacity difference between $\mathbf{H}_{5\text{ray}}$ and $\mathbf{H}_{1\text{ray}}$.

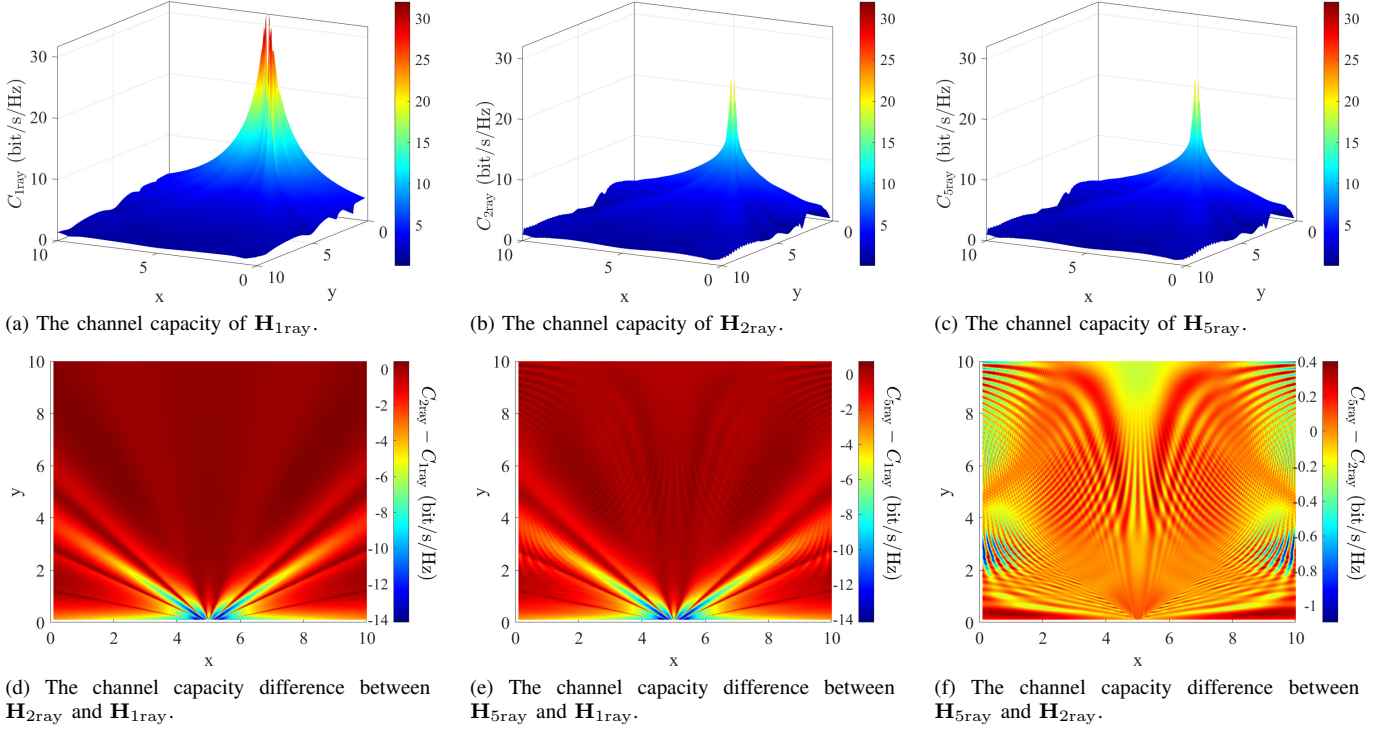(f) The channel capacity difference between $\mathbf{H}_{5\text{ray}}$ and $\mathbf{H}_{2\text{ray}}$.

Fig. 7. Comparisons of the channel capacity of $\mathbf{H}_{1\text{ray}}$, $\mathbf{H}_{2\text{ray}}$, and $\mathbf{H}_{5\text{ray}}$ for wall B, where the incident wave is TE polarised, $\varepsilon_1 = \varepsilon_3 = 2.73 - j0.137$, $[d_1, d_2, d_3] = [12, 96, 12]$ mm.

where $\Re(\cdot)$ and $\Im(\cdot)$ denote the real and imaginary parts of a complex value, respectively, $\Upsilon_{\text{type},m}$, $\Omega_{\text{type},m}$, and $\Xi_{\text{type},m}$ are the typical value ranges of the real part of the relative permittivity, the imaginary part of the relative permittivity, and the thickness of the m-th layer of a sandwich building material, respectively, T_{type} is the minimum required total thickness of the sandwich building material to guarantee its mechanical performance, U_{type} is the maximum allowed thermal transmittance of the sandwich building material to guarantee its thermal performance [40], $\kappa_{\text{type},m}$ denotes the thermal conductivity of the m-th layer of the sandwich building material, and the subscript "type" is either "A" or "B" corresponding to wall A or wall B, respectively. The problem in (23) involves $3M$ optimisation variables.

For the 4-layered wall A shown in Fig. 1(b), the optimisation problem needs to include the following three extra constraints

$$d_2 + d_3 = 31 \text{ mm}, \Re(\varepsilon_2) = 1, \Im(\varepsilon_2) = 0. \quad (24)$$

Hence, the wireless friendliness optimisation for wall A involves 9 variables, i.e., $\Re(\varepsilon_1), \Re(\varepsilon_3), \Re(\varepsilon_4), \Im(\varepsilon_1), \Im(\varepsilon_3), \Im(\varepsilon_4), d_1, d_3, d_4$.

For the 3-layered wall B with a symmetric structure shown in Fig. 1(c), the optimization problem needs to include the following four extra constraints

$$\varepsilon_1 = \varepsilon_3, d_1 = d_3, \Re(\varepsilon_2) = 1, \Im(\varepsilon_2) = 0, \quad (25)$$

Hence, the wireless friendliness optimisation for wall B involves 4 variables, i.e., $\Re(\varepsilon_1), \Im(\varepsilon_1), d_1, d_2$.

B. Iterative algorithm

Since (23) is a non-convex optimisation problem, we propose an iterative algorithm in Algorithm 1 to solve it. The rationale behind Algorithm 1 is to iteratively search through the finite value sets of all the variables in (23) to find the optimal combination of variable values that maximise the spatially averaged capacity. The inputs of Algorithm 1 are as follows: the number of layers M and the type "type" of the sandwich materials, the typical value ranges of the real part of the relative permittivity, $\Upsilon_{\text{type},\{1:M\}}$, the imaginary part of the relative permittivity, $\Omega_{\text{type},\{1:M\}}$, and the thickness, $\Xi_{\text{type},\{1:M\}}$, of the M layers of the sandwich building material, the thermal conductivity of the M layers of the sandwich building material $\kappa_{\text{type},\{1:M\}}$, the minimum required total thickness of the sandwich building material T_{type}, the maximum allowed thermal transmittance of the sandwich building material U_{type}, the number of variables ϖ_{type}, the fixed size of the finite value set of each variable γ, the maximum allowed number of iteration I, and the threshold P_{th} of the relative improvement of the spatially averaged capacity with respect to a benchmark value that will be used to terminate the algorithm.

In Algorithm 1, the concerned ϖ_{type} variables in (23) are arranged in the following order: the M real parts of relative permittivity of the M layers, the M thickness values of the M layers, and the M imaginary parts of relative permittivity of the M layers, and are denoted by $v_1, v_2, ..., v_{\varpi_{\text{type}}}$, where $\varpi_{\text{type}} \leq 3M$. For the jth variable v_j, $\forall j = 1, 2, ..., \varpi_{\text{type}}$, with the minimum $e_j = \min(\cdot)$, the maximum $g_j = \max(\cdot)$, and the incremental step size $f_j = \frac{\max(\cdot) - \min(\cdot)}{\gamma - 1}$, we define its

Algorithm 1: An Iterative Algorithm for Optimising the Wireless Friendliness of a Sandwich Building Material

Input: M, "type", ϖ_{type}, T_{type}, U_{type}, $\Upsilon_{\text{type},\{1:M\}}$, $\Omega_{\text{type},\{1:M\}}$, $\Xi_{\text{type},\{1:M\}}$, $\kappa_{\text{type},\{1:M\}}$, γ, I, P_{th}

1 Collect the set-ups of the MIMO-equipped BS μ, N_{T}, N_{R}, D_0, d_0, ρ_{T} and the parameters of the considered room W, L, X, Y;

2 Arrange the ϖ_{type} variables in the following order: the M real parts of relative permittivity of M layers, the M thickness values of M layers, and the M imaginary parts of relative permittivity of M layers, and denote them by $v_1, v_2, ..., v_{\varpi_{\text{type}}}$;

3 For the jth variable, $\forall j \in \{1, 2, ..., \varpi_{\text{type}}\}$, calculate the minimum, the maximum, and the incremental step size using $e_j = \min(\cdot)$, $g_j = \max(\cdot)$, and $f_j = \frac{\max(\cdot) - \min(\cdot)}{\gamma - 1}$, respectively, and define the finite value set for v_j as $\Phi_j \in \mathbb{R}^{\gamma \times 1} = [e_j : f_j : g_j]$, where "$\cdot$" can be $\Upsilon_{\text{type},m}$ or $\Omega_{\text{type},m}$ or $\Xi_{\text{type},m}$, $\forall m = 1, 2, ..., M, \forall \text{type}$;

4 Initialise $v_1, v_2, ..., v_{\varpi_{\text{type}}}$ and denote them by $v_1^{(0)}, v_2^{(0)}, ..., v_{\varpi_{\text{type}}}^{(0)}$, $i = 0$;

5 Calculate the spatially averaged capacity $C^{(0)} = C_{\text{avg}}\left(v_1^{(0)}, v_2^{(0)}, ..., v_{\varpi_{\text{type}}}^{(0)}\right)$ using (19) and record it as the benchmark: $C_{\text{bench}} = C^{(0)}$;

6 **while** $i \leq I$ **do**

7    $i = i + 1$; $j = 0$;

8   **while** $j \leq \varpi_{\text{type}}$ **do**

9      $j = j + 1$;

10   Calculate $C(V) = C_{\text{avg}}\left(v_1^{(i)}, ..., v_{j-1}^{(i)}, V, v_{j+1}^{(i-1)}, ..., v_{\varpi_{\text{type}}}^{(i-1)}\right)$ using (19) for every $V \in \Phi_j$ that meets both the thickness T_{type} and thermal requirement U_{type};

11      $C_{\text{max,j}}^{(i)} = \max_{V \in \Phi_j} C(V)$;

12   Calculate $P = \frac{\left(C_{\text{max,j}}^{(i)} - C_{\text{bench}}\right)}{C_{\text{bench}}} \times 100\%$;

13   **if** $P \geq P_{\text{th}}$ **then**

14        $v_j^{(i)} = \arg\max_{V \in \Phi_j} C(V)$;

15   Update the benchmark: $C_{\text{bench}} = C_{\text{max,j}}^{(i)}$;

16   **else if** $P < P_{\text{th}}$ and $i \leq 1$ **then**

17        $v_j^{(i)} = v_j^{(i-1)}$;

18   **else if** $P < P_{\text{th}}$ and $i > 1$ **then**

19   **break**;

20 Return the optimised spatially averaged capacity: $\bar{C}_{\text{avg}} = C_{\text{bench}}$;

21 Collect the final values of $v_1, v_2, ..., v_{\varpi_{\text{type}}}$ and denote them by $\bar{v}_1, \bar{v}_2, ..., \bar{v}_{\varpi_{\text{type}}}$;

Output: $\bar{C}_{\text{avg}}, \bar{v}_1, \bar{v}_2, ..., \bar{v}_{\varpi_{\text{type}}}$

TABLE II
PARAMETER SET-UP FOR ALGORITHM 1

Optimisation variant/Parameter	Typical range/Value	Unit
$\Upsilon_{\text{A},4}$	4-7 [32]	-
$\Omega_{\text{A},4}$	0.2-0.6 [32]	-
$\Upsilon_{\text{A},1}$ or $\Upsilon_{\text{B},1}$ or $\Upsilon_{\text{B},3}$	1.5-4.5 [32]	-
$\Omega_{\text{A},1}$ or $\Omega_{\text{B},1}$ or $\Omega_{\text{B},3}$	0.05-0.25 [32]	-
$\Upsilon_{\text{A},3}$	1.2-1.7 [30], [31]	-
$\Omega_{\text{A},3}$	0.2-0.9 [30], [31]	-
T_{A}	193	mm
$\Xi_{\text{A},1}$	5-20	mm
$\Xi_{\text{A},3}$	8-15	mm
$\Xi_{\text{A},4}$	140-190	mm
ϖ_{A}	9	-
T_{B}	120	mm
$\Xi_{\text{B},1}$ or $\Xi_{\text{B},3}$	5-20	mm
$\Xi_{\text{B},2}$	70-110	mm
ϖ_{B}	4	-
I	10	-
P_{th}	1E-6	-
γ	41	-
U_{A}	0.7	$W \cdot m^{-2} \cdot K^{-1}$
U_{B}	0.35	$W \cdot m^{-2} \cdot K^{-1}$
$\kappa_{\text{A},4}$	0.92 [40]	$W \cdot m^{-1} \cdot K^{-1}$
$\kappa_{\text{A},1}$ or $\kappa_{\text{B},1}$ or $\kappa_{\text{B},3}$	0.24 [40]	$W \cdot m^{-1} \cdot K^{-1}$
$\kappa_{\text{A},2}$ or $\kappa_{\text{B},2}$	0.026 [40]	$W \cdot m^{-1} \cdot K^{-1}$
$\kappa_{\text{A},3}$	0.024 [40]	$W \cdot m^{-1} \cdot K^{-1}$

finite value set $\Phi_j \in \mathbb{R}^{\gamma \times 1} = [e_j : f_j : g_j]$, where "$\cdot$" can be $\Upsilon_{\text{type},m}$ or $\Omega_{\text{type},m}$ or $\Xi_{\text{type},m}$, $\forall m = 1, 2, ..., M, \forall \text{type}$. Let $v_j^{(i)}$ denote the jth variable at the ith iteration for $i = 1, 2, ..., I$ and $j = 1, 2, ..., \varpi_{\text{type}}$. The iteration terminates when the relative improvement of the spatially averaged capacity with respect to a benchmark value falls below the threshold P_{th}. Letting I_0 and J_0 denote the final values of i and j, respectively, when the iterative algorithm terminates, then Algorithm 1 alternates the concerned optimisation variables in (23) for a total of $I_0 \varpi_{\text{type}} + J_0$ times.

The outputs of Algorithm 1 are the optimised values of the spatially averaged capacity $\bar{C}_{\text{avg}}$ and the ϖ_{type} variables $\bar{v}_1, \bar{v}_2, ..., \bar{v}_{\varpi_{\text{type}}}$. The computational complexity of Algorithm 1 is in the order of $O(I\varpi_{\text{type}}\gamma)$. The outcomes of our proposed Algorithm 1 are reusable, for example, the output values can be applied to the building materials in several rooms of similar size, shape, and functionality in typical office buildings. Besides, as will be shown in the following simulation results, the proposed Algorithm 1 converges fastly after 3-5 times of iteration, which is easy to implement.

C. Simulation results of Algorithm 1

In the following, we present the simulation results for wall A and wall B using the proposed Algorithm 1. The value/typical ranges of inputs are given in Table II. The other parameters are assumed to be the same as in Fig. 6 and Fig. 7. Except the heat insulation layer, the relative permittivities of other layers of the sandwich building material are initialised with the ITU recommended values, which is calculated by the curve-fitting function of frequency [32, Table 3]. The relative permittivity of the heat insulation layer is given as the medium of its range shown in Table II. The thickness of all layer of the sandwich building material are initialised with the typical values shown
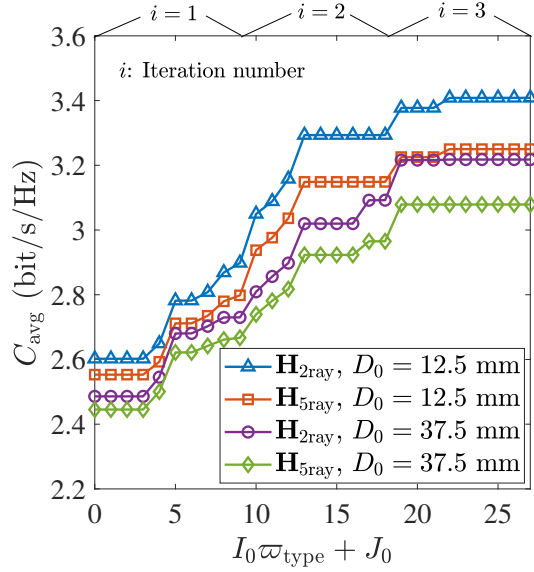
Fig. 8. Spatially averaged capacity versus $I_0\varpi_{\text{type}} + J_0$ for wall A, where $D_0 = 12.5$ mm and $D_0 = 37.5$ mm.

Fig. 9. Spatially averaged capacity versus $I_0\varpi_{\text{type}} + J_0$ for wall B, where $D_0 = 12.5$ mm and $D_0 = 37.5$ mm.

in Fig. 1. The spatially averaged capacity calculated by the initialised thickness and relative permittivities of all layers of the sandwich building material are recorded as the benchmark at the 0th iteration $C^{(0)}$.

Fig. 8 presents the convergence behaviour of the spatially averaged capacity for wall A using Algorithm I based on channel model $\mathbf{H}_{2\text{ray}}$ and $\mathbf{H}_{5\text{ray}}$, respectively, where the distance from the BS to the wall is 12.5 mm and 37.5 mm. The thickness and relative permittivity of each layer are initialised as: $[d_1, d_2, d_3, d_4] = [12, 20, 11, 160]$ mm; $[\Re(\varepsilon_1), \Re(\varepsilon_2), \Re(\varepsilon_3), \Re(\varepsilon_4)] = [2.73, 1, 1.45, 5.24]$; $[\Im(\varepsilon_1), \Im(\varepsilon_2), \Im(\varepsilon_3), \Im(\varepsilon_4)] = [0.137, 0, 0.55, 0.562]$.

As shown in Fig. 8, for the 12.5-mm BS-wall spacing, after 3 times of iteration, the spatially averaged capacity based on $\mathbf{H}_{2\text{ray}}$ increases from 2.60 bit/s/Hz to 3.41 bit/s/Hz, improving 30.98%, while the spatially averaged capacity based on $\mathbf{H}_{5\text{ray}}$ increases from 2.55 bit/s/Hz to 3.25 bit/s/Hz, improving 27.29%. We find that the optimised parameters of wall A are the same for either using spatially averaged capacity based on $\mathbf{H}_{2\text{ray}}$ or using spatially averaged capacity based on $\mathbf{H}_{5\text{ray}}$ as the metric for evaluating and optimising the wireless friendliness of a sandwich building material, which are given as follows: $[d_1, d_2, d_3, d_4] = [6.5, 16, 15, 160]$ mm; $[\Re(\varepsilon_1), \Re(\varepsilon_2), \Re(\varepsilon_3), \Re(\varepsilon_4)] = [4.5, 1, 1.7, 6.85]$; $[\Im(\varepsilon_1), \Im(\varepsilon_2), \Im(\varepsilon_3), \Im(\varepsilon_4)] = [0.05, 0, 0.2, 0.2]$.

As shown in Fig. 8, for the 37.5-mm BS-wall spacing, after 3 times of iteration, the spatially averaged capacity based on $\mathbf{H}_{2\text{ray}}$ is lifted from 2.49 bit/s/Hz to 3.22 bit/s/Hz, improving 29.45%, while the spatially averaged capacity based on $\mathbf{H}_{5\text{ray}}$ is lifted from 2.45 bit/s/Hz to 3.08 bit/s/Hz, improving 25.91%. The optimised parameters are found to be the same for either using spatially averaged capacity based on $\mathbf{H}_{2\text{ray}}$ or using spatially averaged capacity based on $\mathbf{H}_{5\text{ray}}$ as the metric for evaluating and optimising the wireless friendliness of a sandwich building mate-
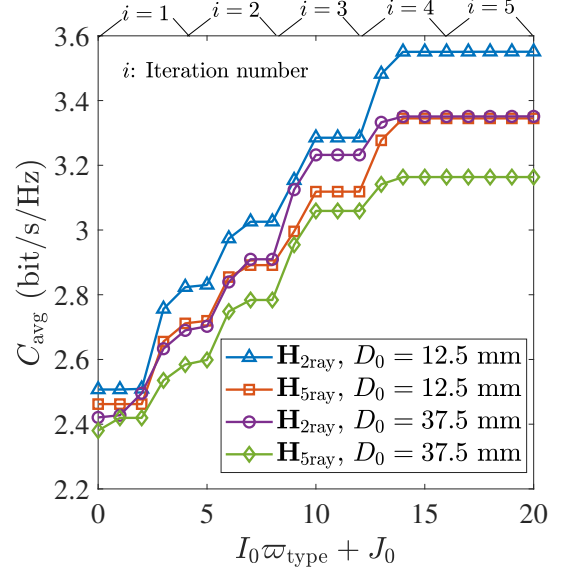
rial, which are given as: $[d_1, d_2, d_3, d_4] = [6.9, 16, 15, 160]$ mm; $[\Re(\varepsilon_1), \Re(\varepsilon_2), \Re(\varepsilon_3), \Re(\varepsilon_4)] = [4.5, 1, 1.7, 6.85]$; $[\Im(\varepsilon_1), \Im(\varepsilon_2), \Im(\varepsilon_3), \Im(\varepsilon_4)] = [0.05, 0, 0.2, 0.2]$.

Fig. 9 shows the convergence behaviour of the spatially averaged capacity for wall B using Algorithm I based on channel model $\mathbf{H}_{2\text{ray}}$ and $\mathbf{H}_{5\text{ray}}$, respectively, where the distance from the BS to the wall is 12.5 mm and 37.5 mm. The real permittivity and thickness of each layer are initialised as: $[\Re(\varepsilon_1), \Re(\varepsilon_2), \Re(\varepsilon_3)] = [2.73, 1, 2.73]$; $[\Im(\varepsilon_1), \Im(\varepsilon_2), \Im(\varepsilon_3)] = [0.137, 0, 0.137]$; $[d_1, d_2, d_3] = [12, 96, 12]$ mm.

As shown in Fig. 9, for the 12.5-mm BS-wall spacing, after 4 times of iteration, the spatially averaged capacity based on $\mathbf{H}_{2\text{ray}}$ is lifted from 2.51 bit/s/Hz to 3.55 bit/s/Hz, improving 41.63%, while the spatially averaged capacity based on $\mathbf{H}_{5\text{ray}}$ is lifted from 2.46 bit/s/Hz to 3.34 bit/s/Hz, improving 35.86%. We find that the obtained optimisation parameters of wall B are the same for both using spatially averaged capacity based on $\mathbf{H}_{2\text{ray}}$ and using spatially averaged capacity based on $\mathbf{H}_{5\text{ray}}$ as the metric for evaluating and optimising the wireless friendliness of a sandwich building material, which are given as: $[\Re(\varepsilon_1), \Re(\varepsilon_2), \Re(\varepsilon_3)] = [4.5, 1, 4.5]$; $[\Im(\varepsilon_1), \Im(\varepsilon_2), \Im(\varepsilon_3)] = [0.05, 0, 0.05]$; $[d_1, d_2, d_3] = [7.3, 110, 7.3]$ mm.

As shown in Fig. 9, for the 37.5-mm BS-wall spacing, after 4 times of iteration, the spatially averaged capacity based on $\mathbf{H}_{2\text{ray}}$ increases from 2.42 bit/s/Hz to 3.35 bit/s/Hz, improving 38.43%, while the spatially averaged capacity based on $\mathbf{H}_{5\text{ray}}$ increases from 2.38 bit/s/Hz to 3.16 bit/s/Hz, improving 32.92%. The obtained optimisation parameters of wall B are the same for both using spatially averaged capacity based on $\mathbf{H}_{2\text{ray}}$ and using spatially averaged capacity based on $\mathbf{H}_{5\text{ray}}$ as the metric for evaluating and optimising the wireless friendliness of a sandwich building material, which are given as: $[\Re(\varepsilon_1), \Re(\varepsilon_2), \Re(\varepsilon_3)] = [4.5, 1, 4.5]$; $[\Im(\varepsilon_1), \Im(\varepsilon_2), \Im(\varepsilon_3)] = [0.05, 0, 0.05]$; $[d_1, d_2, d_3] = [7.3, 110, 7.3]$ mm.

Note that, for the BS-wall distance of 12.5 mm and 37.5 mm, the optimised real parts and imaginary parts of the relative permittivities of all layers of wall A or wall B output from Algorithm I are the same, and the optimised thickness of most layers of wall A or wall B output from Algorithm I are the same, while there is little difference in the optimised thickness of a small amount of layers, which indicates the distance between the BS and the sandwich building material does not affect much the optimised relative permittivites and thickness of the sandwich building material.

Besides, for a specific sandwich material, e.g., either wall A or wall B, the relative improvement of the finalised value $\bar{C}_{\text{avg}}$ with respect to the initialised value $C^{(0)}$ of the spatially averaged capacity decreases with the BS-wall distance. This is intuitive because the effect of the EM properties of a sandwich material will affect the indoor capacity more substantially when it is closer to the BS.

Comparing the relative improvement of the finalised value $\bar{C}_{\text{avg}}$ with respect to the initialised value $C^{(0)}$ in Fig. 8 and Fig. 9, we can see that, with the same BS-wall spacing, the room whose BS's nearest sandwich material is wall B has greater potential improvement in the spatially averaged capacity than the room whose BS's nearest sandwich material is wall A. That is because as the layers of a sandwich building material decreases, the value of the relative permittivity and thickness of each layer of the material affects the indoor wireless capacity more significantly.

V. Conclusion

In this work, we have developed approaches to evaluating and optimising the wireless friendliness of a sandwich building material. First, we have derived and analysed the equivalent reflection coefficient of a sandwich building material for indoor office scenarios, for both TE and TM polarised EM waves. Next, based on a multipath channel model incorporating the LOS path and the WR path from the sandwich building material, we have proposed a metric for evaluating the wireless friendliness of a sandwich building material, i.e., the spatially averaged capacity over a room. Finally, in order to optimise the wireless friendliness of a sandwich material, we have proposed an iterative algorithm to maximise the spatially averaged capacity by jointly optimising the relative permittivity and thickness of each layer of the sandwich material, under the premise of ensuring its mechanical and thermal insulation requirements. The proposed Algorithm 1 can be used to appropriately select the relative permittivities and thickness of all layers of a sandwich building material during the building design and planning stage.

From the numerical results, we have obtained the following insights:

- The variation in the equivalent reflection coefficient of a sandwich building material versus the incident angle becomes more drastic as the number of layers decreases, as shown in Section II-B.
- The incident EM wave polarisation affects the equivalent reflection coefficient of a sandwich building material. For the non-ionised and non-magnetic materials considered

in this work, i.e., wall A and wall B, the TE polarised incident wave results in a larger reflection coefficient amplitude than the TM polarised incident wave, as shown in Section II-B.

- The EM properties and layer structure of a sandwich building material on indoor wireless capacity is non-negligible, especially when the BS is in the vicinity of a surrounding wall. The interference between the LOS path and the WR path from the wall closest to the BS would be much stronger than the interference between the LOS path and the WR paths reflected from the other 3 walls, as shown in Section III-B.
- The relative permittivity and thickness of each layer of a sandwich building material can be jointly adjusted/designed to achieve a 25-42% increase in the spatially averaged capacity, as compared with the benchmark sandwich building material that adopts the relative permittivities given in ITU recommendations and the typical thickness, as shown in Section IV-C.
- For a specific sandwich building material, the relative improvement of the spatially averaged capacity with respect to the initialised value that can be achieved by the proposed Algorithm 1 decreases with the distance between the BS and the wall, which means that more substantial indoor capacity gain can be expected when the BS is deployed closer to a wall, as shown in Section IV-C.
- The relative improvement of the spatially averaged capacity with respect to the initialised value that can be achieved by the proposed Algorithm 1 decreases with the minimum required total thickness of the sandwich building material, which means that more substantial indoor capacity gain can be expected when the sandwich building material under design has less layers, as shown in Section IV-C.
- The distance between the BS and the sandwich building material does not affect much the optimised values of the relative permittivity and thickness of all layers of the sandwich building material, as shown in Section IV-C.

Therefore, it is strongly recommended to appropriately select and/or design the relative permittivities and thickness of each layer of a sandwich building material during building design and planning stage.

Appendix A

For brevity, the variables denoting the UE location (x_a, y_b) are dropped in the following expressions. Following [12, Theorem 2], the ergodic capacity for a certain UE location is given by

$$
C = \kappa \sum_{j=1}^{q} \left(\sum_{i=1}^{q-2} \frac{(\vartheta-1)!}{(G_{i,j})^{-1}} \sum_{k=1}^{\vartheta} E_{\vartheta-k+1}\left(\frac{K_0 S+1}{\rho/N_{\text{T}}}\right) \right.
$$
$$
\left. + \sum_{p=0}^{\infty} \frac{\left(G_{q-1,j}\phi_{q-1}^p + G_{q,j}\phi_q^p\right)}{p!(t-q+p)!((\tau-1)!(t-q)!)^{-1}} \sum_{k=1}^{\tau} E_{\tau-k+1}\left(\frac{K_0 S+1}{\rho/N_{\text{T}}}\right) \right),
$$
$$\tag{26}$$

where $q = \min\{N_R, N_T\}$, and $t = \max\{N_R, N_T\}$, $\vartheta = t - q + j + i - 1$, $\tau = t - q + j + p$, $E_Q(x) = \int_1^\infty e^{-xt} t^{-Q}\, \mathrm{d}t$ denotes the exponential integral,

$$\rho = \frac{(K_0 S + 1)\,\mu^2 \rho_T}{K_0 (4\pi D_1)^2}, \tag{27}$$

in which $\rho_T = \frac{\mathbb{E}(\|\mathbf{x}\|^2)}{\mathbb{E}(\|\mathbf{n}\|^2)}$ denotes the signal-to-noise ratio (SNR) at the BS array,

$$\kappa = \frac{\exp\left(\frac{K_0 S + 1}{\rho / N_T} - \phi_q - \phi_{q-1}\right)}{\ln 2\, ((t-q)!)^{q-1} (\phi_q \phi_{q-1})^{q-2} (\phi_q - \phi_{q-1}) \prod_{l=0}^{q-3} l!}, \tag{28}$$

ϕ_{q-1} and ϕ_q are the two non-zero eigenvalues of $(\mathbf{H_1} + \mathbf{H_2})$ and are given by [12]

$$\phi_{q-1} = \frac{K_0 D_1^2 N_T N_R}{2} \left(\|\mathbf{X}\|^2 - \sqrt{\|\mathbf{X}\|^4 - 4|\det(\mathbf{X})|^2} \right), \tag{29}$$

$$\phi_q = \frac{K_0 D_1^2 N_T N_R}{2} \left(\|\mathbf{X}\|^2 + \sqrt{\|\mathbf{X}\|^4 - 4|\det(\mathbf{X})|^2} \right), \tag{30}$$

$$\mathbf{X} = \begin{bmatrix} \frac{1}{D_1} e^{-j\frac{2\pi D_1}{\mu}} + \frac{\Gamma\Delta\beta\Delta\alpha}{D_2} e^{-j\frac{2\pi D_2}{\mu}} & \frac{\Gamma\Delta\beta\|\mathbf{h}_\alpha\|}{D_2} e^{-j\frac{2\pi D_2}{\mu}} \\ \frac{\Gamma\Delta\alpha\|\mathbf{h}_\beta\|}{D_2} e^{-j\frac{2\pi D_2}{\mu}} & \frac{\Gamma\|\mathbf{h}_\alpha\|\|\mathbf{h}_\beta\|}{D_2} e^{-j\frac{2\pi D_2}{\mu}} \end{bmatrix}, \tag{31}$$

$$[\mathbf{h}_\alpha]_{n_T} = \frac{e^{-j\left(n_T - 1 - \frac{N_T - 1}{2}\right)\alpha_2} - \Delta\alpha\, e^{-j\left(n_T - 1 - \frac{N_T - 1}{2}\right)\alpha_1}}{\sqrt{N_T}}, \tag{32}$$
$$\text{for } n_T \in \{0, 1, ..., N_T - 1\},$$

$$[\mathbf{h}_\beta]_{n_R} = \frac{e^{-j\left(n_R - 1 - \frac{N_R - 1}{2}\right)\beta_2} - \Delta\beta\, e^{-j\left(n_R - 1 - \frac{N_R - 1}{2}\right)\beta_1}}{\sqrt{N_R}}, \tag{33}$$
$$\text{for } n_R \in \{0, 1, ..., N_R - 1\},$$

$$\Delta\beta = \frac{\sin\left(N_R (\beta_1 - \beta_2)/2\right)}{N_R \sin\left((\beta_1 - \beta_2)/2\right)}, \tag{34}$$

$$\Delta\alpha = \frac{\sin\left(N_T (\alpha_1 - \alpha_2)/2\right)}{N_T \sin\left((\alpha_1 - \alpha_2)/2\right)}, \tag{35}$$

and $G_{i,j}$ is the (i,j)th-co-factor of the $q \times q$ matrix $\mathbf{Z}$ whose (l,k)th entry is given by

$$[\mathbf{Z}]_{l,k} = \begin{cases} (t - q + k + l - 2)!, & 1 \le l \le q - 2, \\ \frac{{}_1 F_1(t-q+l, t-q+1, \phi_k)}{[(t-q+l-1)!]^{-1}}, & \text{otherwise}, \end{cases} \tag{36}$$

where ${}_1 F_1(e, o, g) = \sum_{s=0}^\infty \frac{[e]_s g^s}{[o]_s s!}$ denotes the hypergeometric function, $[r]_t = \frac{(r+t-1)!}{(r-1)!}$, and $(\cdot)!$ denotes the factorial function.

REFERENCES

[1] Y. Yao, Y. Shao, J. Zhang and J. Zhang, "A transparent antenna using metal mesh for UWB MIMO applications," *IEEE Trans. Anten. and Propag.*, vol. 71, no. 5, pp. 3836-3844, May 2023.

[2] A. A. Ayeni, A. A. Yusuf and S. O. Onidare, "Correlation between the electromagnetic properties of building materials and wireless signal penetration loss," *IEEE Trans. Anten. and Propag.*, vol. 70, no. 12, pp. 12040-12048, Dec. 2022.

[3] 5G PPP Technology Board. "Delivery of 5G services indoors—The wireless wire challenge and solutions." Sep. 2021. [Online]. Available: https://5g-ppp.eu/wp-content/uploads/2021/09/Delivery-of-5G-servicesindoors-v1.0-final-2.pdf

[4] D. Shakya, *et al.*, "Dense urban outdoor-indoor coverage from 3.5 to 28 GHz," *ICC 2022 - IEEE International Conference on Communications*, Seoul, Korea, Republic of, 2022, pp. 932-937.

[5] Aragón-Zavala, Alejandro. "Indoor wireless communications: from theory to implementation," *John Wiley & Sons*, Incorporated, 2017.

[6] J. Zhang, *et al.*, "Fundamental wireless performance of a building," *IEEE Wirel. Commun.*, vol. 29, no. 1, pp. 186–193, Apr. 2021.

[7] J. Zhang, A. A. Glazunov and J. Zhang, "Wireless performance evaluation of building layouts: closed-form computation of figures of merit," *IEEE Trans. Commun.*, vol. 69, no. 7, pp. 4890-4906, Jul. 2021.

[8] Y. Huang, J. Zhang, and J. Zhang, "Wireless channel delay spread performance evaluation of a building layout,", *IEEE Trans. Veh. Technol.*, early access, 2022.

[9] J. Lin, *et al.*, "Evaluation of building wireless performance for indoor device-to-device networks," *IEEE Trans. Green Commun. and Network.*, early access, 2023.

[10] C. Chen, *et al.*, "On the performance of indoor multi-story small-cell networks," *IEEE Trans. Wirel. Commun.*, vol. 20, no. 2, pp. 1336-1348, Feb. 2021.

[11] D. Chizhik, J. Du and R. A. Valenzuela, "Universal path gain laws for common wireless communication environments," *IEEE Trans. Anten. and Propag.*, vol. 70, no. 4, pp. 2928-2941, Apr. 2022.

[12] Y. Zhang, *et al.*, "How friendly are building materials as reflectors to indoor LOS MIMO communications?," *IEEE Internet Things J.*, vol. 7, no. 9, pp. 9116-9127, Sept. 2020.

[13] Y. Zhang, J. Zhang, X. Chu, and J. Zhang, "Lower-bound capacity based wireless friendliness evaluation for walls as reflectors," *IEEE Trans. Broadcast.*, vol. 67, no. 4, pp. 917-924, Dec. 2021.

[14] Y. Zhou, Y. Shao, J. Zhang and J. Zhang, "Wireless performance evaluation of building materials integrated with antenna arrays," *IEEE Commun. Lett.*, vol. 26, no. 4, pp. 942-946, Apr. 2022.

[15] Y. Zhang, "Wireless friendliness evaluation of building materials as reflectors," Ph.D. Thesis, University of Sheffield, May 2022.

[16] Y. Zhang, *et al.*, "Effects of wall reflection on the per-antenna power distribution of ZF-precoded ULA for indoor mmWave MU-MIMO transmissions," *IEEE Commun. Lett.*, vol. 25, no. 1, pp. 13-17, Jan. 2021.

[17] Y. Huang, J. Zhang and J. Zhang, "Building wireless performance evaluation of channel hardening for massive MIMO system," *IEEE Commun. Lett.*, vol. 27, no. 7, pp. 1874-1878, Jul. 2023.

[18] K. Haneda, *et al.*, "Indoor 5G 3GPP-like channel models for office and shopping mall environments," *IEEE International Conference on Communications Workshops (ICC)*, Kuala Lumpur, 2016, pp. 694-699.

[19] S. K. Yoo, *et al.*, "Ceiling- or wall-mounted access points: an experimental evaluation for indoor millimeter wave communications," *13th European Conference on Antennas and Propagation (EuCAP)*, Krakow, Poland, 2019, pp. 1-5.

[20] W. Yang, *et al.*, "Measurements of reflection and penetration loss in indoor environments in the 39-GHz band," *15th European Conference on Antennas and Propagation (EuCAP)*, 2021, pp. 1-5.

[21] Y. Ai, J. B. Andersen and M. Cheffena, "Path-loss prediction for an industrial indoor environment based on room electromagnetics," *IEEE Trans. on Anten. Propag.*, vol. 65, no. 7, pp. 3664-3674, Jul. 2017.

[22] Y. Wang et al., "Measured reflection and transmission properties of building materials for indoor THz communication," *IEEE Anten. and Wireless Propag. Lett.*, vol. 22, no. 6, pp. 1361-1365, Jun. 2023.

[23] N. Hosseini et al., "Attenuation of several common building materials: millimeter-wave frequency bands 28, 73, and 91 GHz," *IEEE Anten. and Propag. Mag.*, vol. 63, no. 6, pp. 40-50, Dec. 2021.

[24] A. Asp, *et al.*, "Impact of different concrete types on radio propagation: fundamentals and practical RF measurements," *4th International Conference on Smart and Sustainable Technologies (SpliTech)*, Split, Croatia, 2019, pp. 1-8.

[25] A. Asp, *et al.*, "Impact of concrete moisture on radio propagation: fundamentals and measurements of concrete samples," *16th International Symposium on Wireless Communication Systems (ISWCS)*, Oulu, Finland, 2019, pp. 542-547.

[26] R. Rudd, *et al.*, "Building materials and propagation: final report," Sep. 2014. [Online]. Available: https://www.ofcom.org.uk/_data/assets/pdf_file/0016/84022/building_materials _and_propagation.pdf
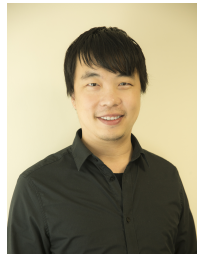
[27] K. Sato et al., "Measurements of reflection and transmission characteristics of interior structures of office building in the 60-GHz band," *IEEE Trans. on Anten. and Propag.*, vol. 45, no. 12, pp. 1783-1792, Dec. 1997.

[28] Y. C. Lee, S. -S. Oh, C. W. Byeon, K. Aziding and B. -L. Cho, "Impact of window penetration loss on building entry loss from 3.5 to 24 GHz," *IEEE Access*, vol. 9, pp. 138571-138579, 2021.

[29] S. Gerges, P. Gkorogias, "Concrete sandwich element design in terms of passive housing recommendations and moisture safety," Master Thesis in Building Technology, KTH Architecture and the Built Environment.

[30] C. Eyraud, *et al.*, "Complex permittivity determination from far-field scattering patterns," *IEEE Antennas Wirel. Propag. Lett.*, vol. 14, pp. 309-312, 2015.

[31] S. B. Bibikov, *et al.*, "Some approaches to the development of absorbing materials for ultrawideband systems," *5th International Conference on Ultrawideband and Ultrashort Impulse Signals*, Sevastopol, Ukraine, 2010, pp. 262-265.

[32] ITU-R, "Effects of building materials and structures on radiowave propagation above about 100 MHz P series radiowave propagation," *Recomm. ITU-R P.2040-2*, Sep. 2021.

[33] S. S. Zhekov, O. Franek and G. F. Pedersen, "Dielectric properties of common building materials for ultrawideband propagation studies [Measurements corner]," *IEEE Antenn. and Propag. Mag.*, vol. 62, no. 1, pp. 72-81, Feb. 2020.

[34] P. D. Jensen, et al., "Cole–Cole parameter characterization of urea and potassium for improving dialysis treatment assessment," *IEEE Antenn. Wireless Propag. Lett.*, vol. 11, pp. 1598–1601, Jan. 3, 2013.

[35] F. Sagnard and G. E. Zein, "In situ characterization of building materials for propagation modeling: frequency and time responses," IEEE Trans. Antennas Propag., vol. 53, no. 10, pp. 3166-3173, Oct. 2005.

[36] C. Jansen, et al., "The impact of reflections from stratified building materials on the wave propagation in future indoor terahertz communication systems," IEEE Trans. Antennas Propag., vol. 56, no. 5, pp. 1413-1419, May 2008.

[37] D. Pena, et al., "Measurement and modeling of propagation losses in brick and concrete walls for the 900-MHz band," IEEE Trans. Antennas Propag., vol. 51, no. 1, pp. 31-39, Jan. 2003.

[38] M. B. Zetterberg, *et al.*, "IST-2003-507581 WINNER D5.4 v1.4 final report on link level and system level channel models," Nov. 2005.

[39] E. Torkildson, U. Madhow and M. Rodwell, "Indoor millimeter wave MIMO: feasibility and performance," *IEEE Trans. Wirel. Commun.*, vol. 10, no. 12, pp. 4150-4160, Dec. 2011.

[40] J. Willoughby, Plant Engineer's Reference Book (Second Edition), 2002.

Jiliang Zhang (M'15, SM'19) is currently a full Professor at College of Information Science and Engineering, Northeastern University, Shenyang, China. He has pioneered systematic building wireless performance evaluation, modeling, and optimization, with the key concepts summarized in Fundamental Wireless Performance of a Building, IEEE Wireless Communications, 29(1), 2022.

Xiaoli Chu (M'06-SM'15) is a Professor in the Department of Electronic and Electrical Engineering at the University of Sheffield, UK. She received the B.Eng. degree in Electronic and Information Engineering from Xi'an Jiao Tong University in 2001 and the Ph.D. degree in Electrical and Electronic Engineering from the Hong Kong University of Science and Technology in 2005. From 2005 to 2012, she was with the Centre for Telecommunications Research at King's College London. Xiaoli has co-authored over 200 peer-reviewed journal and conference papers, including 8 ESI Highly Cited Papers and the IEEE Communications Society 2017 Young Author Best Paper. She co-authored/co-edited the books "Fog-Enabled Intelligent IoT Systems" (Springer 2020), "Ultra Dense Networks for 5G and Beyond" (Wiley 2019), "Heterogeneous Cellular Networks - Theory, Simulation and Deployment" (Cambridge University Press 2013), and "4G Femtocells: Resource Allocation and Interference Management" (Springer 2013). She is a Senior Editor for the IEEE Wireless Communications Letters and an Associate Editor for the IEEE Transactions on Network Science and Engineering, the IEEE Open Journal of Vehicular Technology, and the IEEE Transactions on Machine Learning in Communications and Networking. She received the IEEE Communications Letters Exemplary Editor Award in 2018.

Yixin Zhang received the B.Eng. degree in electronic and information engineering from Beijing University of Posts and Telecommunications (BUPT), Beijing, China, in 2017, and the Ph.D. degree in electronic and electrical engineering from the University of Sheffield, Sheffield, UK, in 2022. She is currently a Lecturer with the School of Information and Communication Engineering, BUPT, Beijing, China. She was awarded in 2018 a Marie Sklodowska-Curie Fellowship as part of the EU-H2020-ITN funded project 'Mmwave Communications in the Built Environments (WAVECOMBE)'. She has been with Nokia Bell Labs, Espoo, Finland from 2020 to 2022 and Televic Conference, Izegem, Belgium from 2019 to 2020. Her research interests include the smart built environment, intelligent reflective surface, electromagnetic wave propagation, channel characterisation, and MIMO antenna configuration.

Jie Zhang has held the Chair in Wireless Systems at the Department of Electronic and Electrical Engineering, The University of Sheffield, since January 2011. He is also the Founder, Board Director, and Chief Scientific Officer (CSO) of Ranplan Wireless, a public company listed on Nasdaq OMX. Ranplan Wireless produces a suite of world's first joint indoor/outdoor 5G/4G/WiFi network planning and optimization tools suites, including Ranplan Professional and Collaboration-Hub, which are being used by the world's largest mobile operators and network vendors across the globe. Along with his students and colleagues, he has pioneered research in small cell and heterogeneous network (HetNet) and published some of the landmark papers and books on these topics, widely used by both academia and industry. Since 2010, he and his team have also developed ground-breaking work in modeling and designing smart built environments considering both wireless and energy efficiency. His Google Scholar citations are in excess of 7800 with an H-index of 38. Prior to his current appointments, he studied and worked at Imperial College London, University of Oxford, University of Bedfordshire, and East China University of Science and Technology, reaching the rank of a Lecturer, Reader, and Professor in 2002, 2005, and 2006, respectively.